Influence of droplet collision modelling in Euler/Lagrange calculations of spray evolution

S. Lain[1] and M. Sommerfeld[1,2]

[1] PIA+ Group, Department Mechanical Engineering, Universidad Autónoma de Occidente, Cali, Colombia
Email: Santiago.lain@gmail.com

[2] Multiphase Flow Systems (MPS), Institute of Process Engineering, Otto-von-Guericke-University Magdeburg, Hoher Weg 7b, D-06120 Halle (Saale), Germany
Email: martin.sommerfeld@ovgu.de

Graphical Abstract

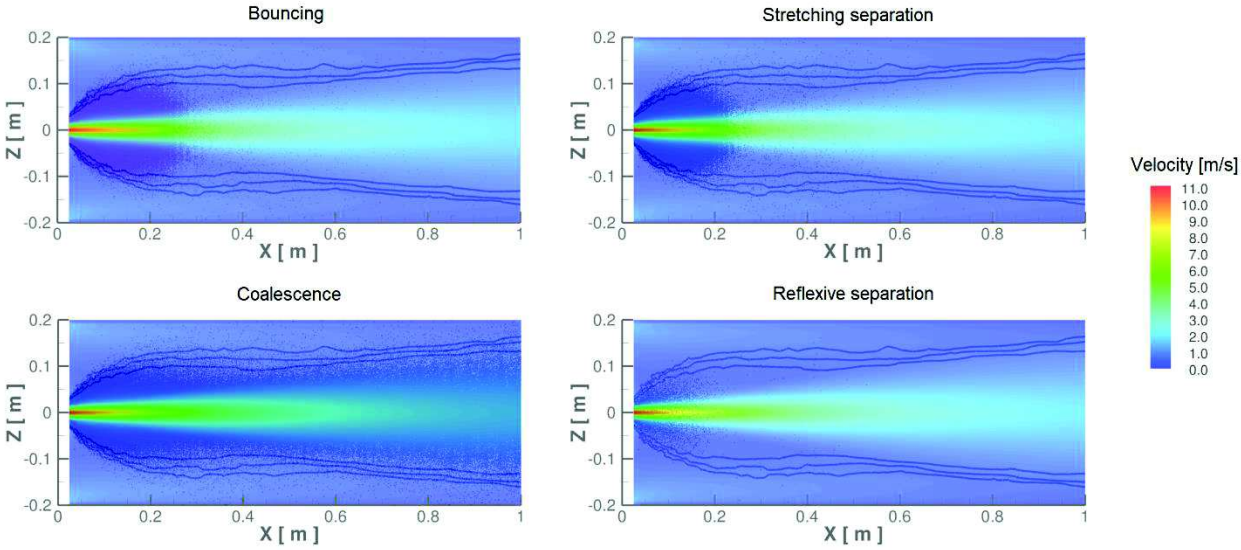

Simulated hollow cone spray structure with gas-phase velocity field (colour coded), spray droplet concentration field indicated by three contour lines (from outer to inner side 3, 5 and 10 g/m^3) and droplet collision locations for bouncing, coalescence, stretching and reflexive separation indicated by black points.

Influence of droplet collision modelling in Euler/Lagrange calculations of spray evolution

S. Lain[1] and M. Sommerfeld[1,2]

[1] PIA+ Group, Department Mechanical Engineering, Universidad Autónoma de Occidente, Cali, Colombia
Email: Santiago.lain@gmail.com

[2] Multiphase Flow Systems (MPS), Institute of Process Engineering, Otto-von-Guericke-University Magdeburg, Hoher Weg 7b, D-06120 Halle (Saale), Germany
Email: martin.sommerfeld@ovgu.de

Abstract

The numerical computation of spraying systems is favourably conducted by applying the Euler/Lagrange approach. Although sprays downstream of the breakup region are very often rather dilute, droplet collisions may still have a significant influence on the spray evolution and especially the produced droplet size spectrum. Consequently, they have to be reliably modelled in the Lagrangian tracking approach. For this purpose, the fully stochastic droplet collision model is applied, which is numerically very efficient. It is demonstrated that this model is largely independent of the considered flow mesh and hence grid size, as well as the number of tracked parcels and the Lagrangian time step size. Moreover, this model includes the impact efficiency which may remarkably reduce collision rates for a wide droplet size spectrum. An essential ingredient of any droplet collision model is the proper description of the collision outcome through the so-called collision maps (i.e. the non-dimensional impact parameter plotted versus collision Weber number; B = f(We)), where the outcome regions (i.e. bouncing, coalescence and stretching or reflexive separation) are demarked by appropriate, mostly theory-based boundary lines. There are a number of different correlations available which may be applied for this purpose. The structure of the collision maps strongly depends on the kind of liquid being atomised. Different types of boundary lines and collision map structures are analysed here in detail with regard to the conditional collision rates or numbers within a rather simple hollow cone spray. The comparison of the averaged Sauter mean diameters along the spray demonstrates the importance of droplet collisions and how strongly this result is affected by the presumed droplet collision maps. Crude approximations to such collision maps may result in large errors and wrong predictions of the produced

droplet size spectrum. Moreover, it is demonstrated that the effective PDF (probability density function) of the colliding droplet size ratio has typically a maximum in the range $0.1 < \Delta < 0.3$, a condition where no experimental data are available so far and some of the commonly used boundary lines are not suitable. Naturally, the spray simulations are compared to experimental data for a water hollow-cone spray, showing excellent agreement if the droplet collision map is selected properly. This concerns profiles of both gas and droplet velocities as well as droplet concentration development and local droplet size distributions. Expectedly, the prediction of the velocities is less sensitive with respect to the presumed droplet collision map.

Keywords: Euler/Lagrange computations; hollow-cone spray; binary droplet collisions; modelling collision outcomes; collision maps; coalescence; bouncing; separation.

1 Introduction

Spraying systems have numerous technical and industrial applications but are also an everyday companion. Examples are spray drying, spray cooling of surfaces and the environment, spray combustion of liquid fuels, spray painting associated with surface coating and numerous kinds of spray cans. All of these processes have different objectives and goals, but a very common one is the production of very fine droplets with a huge volume specific surface area to favour rapid heat and mass transfer as for example in combustion engines. Other processes aim to produce a desired droplet size spectrum in order to produce a powder with desired properties like in spray dryers. Also, the surface coating through spraying systems requires certain droplet sizes in order to yield favourable film thickness and surface structure. As a result of the mostly difficult environment a spray is operated in, such as, spray drying chamber or combustion chamber, an experimental observation and analysis constitutes a huge challenge and is often even impossible (e.g. dense spray region, high temperature and pressure environment). Therefore, numerical computations (CFD-computational fluid dynamics) of spraying systems have become an attractive approach over the past decades. Additionally, this fast development is supported by the growth of computational power and the advances in numerical methods and the mostly required models for unresolved transport processes.

A spray, although from the first glance seems to be very simple, involves a number of sub-processes which require quite sophisticated models, as atomisation of the liquid being determined by the nozzle type, liquid fragment or droplet break-up (i.e. called secondary

breakup), droplet collisions, heat and mass transfer and possibly also droplet-wall collisions with liquid deposition.

In principle there are two ways in numerically describing the behaviour of technical spraying systems, categorised as dispersed multi-phase flow, the continuum approach, often called two-fluid or Euler/Euler method, and the discrete point-particle modelling, called Euler/Lagrange method (see e.g. Kolakaluri et al. 2014, Sommerfeld 2017 a)). In two-fluid modelling approaches the discrete nature of the spray droplets is lost due to the averaging of droplet properties and the interfacial interaction (or coupling) terms between both phases (i.e. air and discrete droplets) within the computational control volumes. Therefore, all transport process occurring on the scale of the droplets have to be described through theoretically derived closures or by additionally plugged-in models, such as a population balance. Advantages of the two-fluid approach are seen in the capturing of the nozzle flow, the liquid sheet or jet breakup and the dense spray region (see e.g. Platzer and Sommerfeld 2006; Sorianao-Palao et al. 2014). The natural way to describe spraying systems is of course the Lagrangian approach which was also applied in the early times to simulate entire sprays, in this case related to combustion (Dukowicz 1980). In order to represent the real number of produced droplets and the correct droplet mass flow rate, the parcel concept was introduced, where each computational particle represents a certain number of reals droplets with the same properties (Dukowicz 1980). This initiation was followed by numerous studies at Los Alamos Laboratories, eventually ending up in the step-by-step extended well-known KIVA-code directed towards the simulation of spray combustion (O`Rourke and Amsden 1987; Amsden et al. 1989). The well-known deterministic-stochastic droplet collision model, still in use today, was developed by O`Rourke (1981). Naturally, also other research groups were involved in initial developments of Lagrangian approaches for spray simulations. Exemplary the thesis of Bauman (2001) should be mentioned which gives a detailed overview of the modelling approaches for the relevant elementary processes being the state-of-the-art at that time. As mentioned above, also in a Lagrangian approach a number of models for the involved unresolved elementary processes are necessary although this approach, as one is moving with the droplets, allows for a more descriptive and mechanistic model development.

Due to these advantages, the Euler/Lagrange approach is mostly applied to simulate different kinds of spraying systems (Fritsching 2004; Woo 2016) and also spray combustion (Merci and Gutheil 2014). The focus of this contribution is on modelling of droplet collisions and their outcomes as well as the resulting droplet size spectrum produced by a spray. In such sprays, where just downstream of the atomisation or break-up region the initial droplet

concentration is quite high, droplet collisions will occur and influence the produced droplet size distribution further downstream (see for example Rüger et al. 2000). The often-dominant collision outcome, namely droplet coalescence, yields an increase of the Sauter mean diameter along the spray, when averaged over the entire spray cross-section (Rüger et al. 2000, Guo et al. 2004). On the other hand, separative droplet collisions are observed causing the formation of fine satellite droplets which cause a reduction of the resulting droplet mean size (Ko und Ryou 2005). Consequently, for a correct prediction of the produced spray droplet size not only atomisation and droplet-break-up have to be modelled properly, but also the occurrence and the outcome of droplet collisions.

Lagrangian droplet collision models

In order to model droplet collisions in the frame of the Lagrangian droplet parcel concept, where only point-masses are tracked, several sub-processes have to be considered (Sommerfeld 2017 b), Sommerfeld and Lain 2017). The first step of the collision model is the detection of the possibility of a collision between two droplets among several hundred thousand of parcels tracked through the computational domain. This may be done in three ways: fully deterministic with geometrical construction of crossing trajectories (Sundaram and Collins 1996), deterministic-stochastic detection model in the frame of the parcel concept (O`Rourke 1981) and fully stochastic detection model where explicitly no information on neighbouring droplets is needed (Sommerfeld 2001). More details on these collision detection approaches are also provided by Sommerfeld and Pasternak (2019). Nowadays, in spray simulations some additional features are considered for improving the classical deterministic-stochastic collision detection of O`Rourke (1981). This is first of all the strong sensitivity of the collision detection on the selected mesh size for flow computations. Such as shortcoming was removed by the so-called “no-time-counter” algorithm introduced by Schmidt and Rutland (2000) or by using a sphere of influence as a search scope for finding collision partners (Guo et al. 2004, Nijdam et al. 2006) or building an adapted collision grid (see e.g. Zhang et al. 2012). Moreover, hybrid models were suggested in order to ensure that the collision partners always move towards each other just prior to collision, as done by Nordin (2001) through an incorporation of a rather expensive droplet tracking collision detection method. A detailed analysis and validation of such hybrid models was conducted by Pischke et al. (2015) followed by guidelines for a proper selection of hybrid droplet collision models.

The applied collision detection model also needs to consider the impact efficiency being relevant for collisions between small and large droplets (Ho and Sommerfeld 2002), whereby the smaller droplets might move around the larger one with the relative flow. Although this is

a situation occurring frequently is sprays due to the wide droplet size spectrum, it has been neglected in most spray simulations so far. It should be emphasised that neglecting impact efficiency the collision rates are remarkably over-predicted (Sommerfeld and Lain 2017). This step includes the determination of the collision point on both droplet surfaces, so that the collision Weber-number, We, and the non-dimensional impact parameter, *B*, can be calculated:

$$We = \frac{\rho\, d_S\, u_{rel}^2}{\sigma} \tag{1}$$

$$B = \frac{2\, b}{d_S + d_L} = sin\, \varphi \tag{2}$$

The collision Weber-number, *We*, is determined with the relative velocity of colliding droplets, u_{rel}, (see Figure 1), the liquid properties (i.e. ρ and σ are the density and surface tension of the fluid) and with the diameter of the smaller droplet d_S. By definition *B* is the sinus of the enclosed angle φ between the relative velocity vector u_{rel} and the position vector P_{SL} between the droplets centre points (see Figure 1). These two parameters are used to create the well-known collision maps (i.e. *B = f(We)*) whereby the different collision outcomes may be identified, such as bouncing, stretching separation, coalescence and reflexive separation (see Figure 2). Moreover, the Ohnesorge-number *Oh*, being characterised by the liquid properties, including the liquid viscosity μ together with the droplet diameter, mostly the small droplet diameter d_S, is very often helpful since it is independent of the relative velocity. An additional geometrical parameter especially for sprays, is of course the droplet size ratio Δ.

$$O\square = \frac{\mu}{\sqrt{\rho\ \sigma\ d_S}} \tag{3}$$

$$\Delta = \frac{d_S}{d_L} \tag{4}$$

From these numbers one may derive also other non-dimensional parameters which are useful to characterise the collision process in different ways (see e.g. Sommerfeld and Kuschel 2016), being the Reynolds-number *Re* and the Capillary-number *Ca*:

$$Re = \frac{\sqrt{We}}{Oh} = \frac{\rho\ d_S\ u_{rel}}{\mu} \tag{5}$$

$$Ca = O\square\ \sqrt{We} = \frac{\mu}{\sigma} u_{rel} = \frac{u_{rel}}{u_{relax}} \tag{6}$$

here $u_{relax} = \sigma/\mu$ is the relaxation velocity often used to describe plastic deformations.

In case the colliding droplets are carrying different liquids, additional non-dimensional parameters have to be considered, such as ratios of viscosity and surface tension as well as liquid density.

The next step in the collision model is the identification of the collision scenario and the outcome on the basis of the well-known collision maps, i.e. $B = f(We)$, as illustrated in Figure 2. The decision about which type of collision is occurring (i.e. bouncing, coalescence or stretching and reflexive separation) is based on analytical or theoretical derived boundary lines indicated by the lines in Figure 2. The properties of the newly formed droplets depend on the collision type at hand and have to be calculated based on mass and momentum balances (i.e. number of droplets, droplet sizes and their new velocities). Most of the numerical computations of spraying systems or the interaction between two sprays use the deterministic-stochastic collision detection model of O`Rourke (1981).

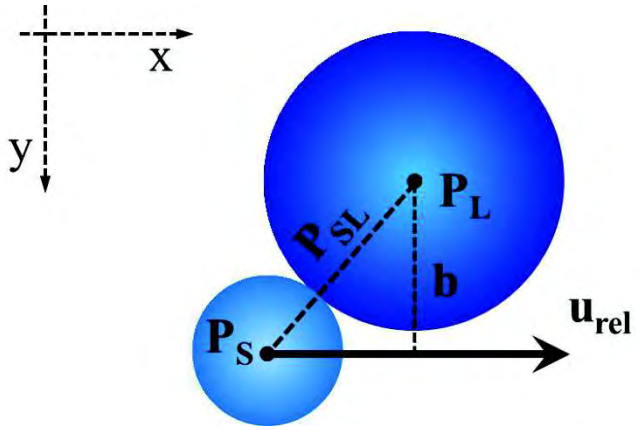

Figure 1: Geometry of binary droplet collision with different sized droplets, P_S and P_L indicate the centroids of both droplets, b is the lateral displacement and u_{rel} the relative velocity in the collision plane x-y, aligned with the collision cylinder axis.

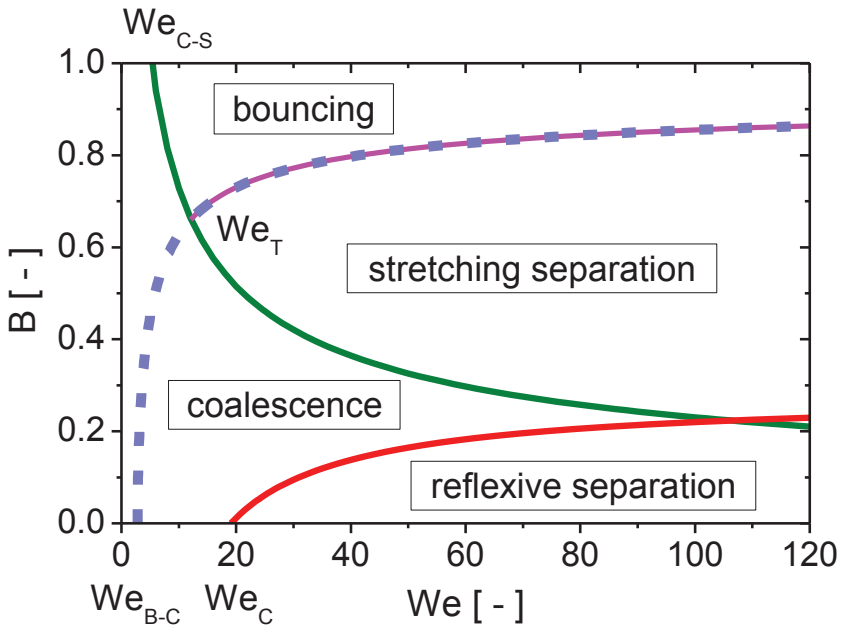

Figure 2: Typical droplet collision map where the non-dimensional impact parameter B is plotted versus collision Weber-number, *We*, including typical boundary lines between collision outcomes and four characteristic points, specified with the relevant We-number (source: Sommerfeld and Pasternak 2019).

The collision maps as illustrated in Figure 2 are being used for many years to classify the outcomes of binary droplet collisions. In the lower We-regime, which is considered here (i.e. $We < 200$), one can distinguish between bouncing, coalescence, stretching and reflexive separation. These different regimes are demarked by boundary lines either determined experimentally or theoretically. These boundary lines are the lower limit of bouncing (B), stretching separation-coalescence (SS-C) and reflexive separation-coalescence (RS-C). The most common boundary models were summarized and analysed by Sommerfeld and Pasternak (2019). Characteristic points in this kind of collision map are transition from bouncing to coalescence, called $We_{B\text{-}C}$, the critical Weber-number We_C, the triple point location We_T and for special cases the transition from coalescence to bouncing, called $W_{C\text{-}S}$ (see Figure 2).

Some years back, droplet collision outcomes are only modelled by distinguishing between coalescence and grazing (grazing combines bouncing and stretching separation in Figure 2) collision (see e.g. Gavaises et al. 1996, Rüger et al. 2000, Guo et al. 2004, Nijdam et al. 2006). Actually, this boundary line goes also back to the work of O`Rourke (1981) which was termed coalescence efficiency in this work and specifies the critical impact parameter B^* below which coalescence occurs (see closed line in Figure 2 going through $W_{C\text{-}S}$). The associated correlation was derived based on theory and measurements of Brazier-Smith et al. (1972). In these single-boundary-line models only coalescence and grazing are considered as an outcome, where grazing implies that the two droplets continue their direction of motion after collision, but with reduced velocity magnitude due to dissipation (O`Rourke 1981). Mostly grazing is modelled without satellite formation with the argument that their mass is negligibly small. All other collision outcomes (e.g. reflexive separation or shattering) are neglected including also satellite formation. Such a single boundary line is generally only suitable for water where bouncing is not found in the region of small We over the entire B-regime, or milk spray which does not show bouncing at all (Finotello et al. 2019), but still, reflexive separation is not considered, whereby the occurrence of coalescence is overestimated. Such a single-line boundary model is of course not suitable for many other liquids a mentioned above (see also Sommerfeld and Pasternak 2019). Especially for simulating diesel or fuel sprays there should be at least 3 boundary lines considered, namely, bouncing, SS-C and RS-C.

Spray simulations

In the numerical computations of Post and Abraham (2002) for Diesel spray injection, the collision outcome was described by considering all collision scenarios. Hence, a hybrid model was used combining the boundary models of Estrade et al. (1999) for defining the lower boundary of bouncing, the Brazier-Smith et al. (1972) model for specifying the coalescence efficiency (i.e. upper boundary of coalescence) and the Ashgriz and Poo (1990) model to define the region of reflexive separation. Formation of smaller satellite droplets due to shattering collision was only considered to occur (Post and Abraham 2002). A comparison of the results obtained with the single-line and the composite model showed of course completely different fractions for the collision outcomes. For the single-line model they found 53% coalescence and 47% grazing or stretching separation. The three-line model yielded much lower coalescence fractions, only 5%, whereas bouncing without size change constitutes now a fraction of 78%. The portion of stretching separation was 16%, while reflexive separation amounted only 1%, may be the result of the combination of low B and high We. Consequently, the structure of the considered collision map has an immense influence on the produced droplet size and hence the spray behaviour. It was shown that when solely applying the Brazier-Smith et al. (1972) model the Sauter mean diameter along the spray increases at a much higher rate compared to the proposed composite three-line model, which is of course provoked by the drastic decrease of the coalescence fraction. Additionally, it was shown that the grid resolution has a remarkable effect on the computed collision rates, being much higher for finer meshes. This might be associated with a better resolution of flow and turbulence properties seen by the droplets. On the other hand, it is known that the collision rate obtained by the O`Rourke (1981) collision model itself is depending in grid size, but here a finer mesh would result in lower collision rates. As a result, for a too coarse mesh the development of the Sauter mean diameter in time is not predicted correctly.

However, one must state that collision maps and boundary lines obtained for “water” (note that here only the Estrade et al. (1999) boundary line is obtained for Ethanol) are not suitable for calculations of a Diesel sprays due to the large sensitivity of the results. As illustrated in Figure 10 of Post and Abraham (2002) the boundary lines for the model fuel tetradecane (Qian and Law 1997) are completely different than those for water. They are remarkably shifted to higher We-numbers (i.e. due to viscosity increase) whereby it cannot be expected that a diesel spray is correctly predicted with water boundary lines (Post and Abraham 2002). A comparison with measurements was unfortunately not performed. In the composite droplet collision model used by Kollar et al. (2005) the same collision outcomes

and the same boundary lines were considered, again neglecting satellite formation after separation.

The composite collision model used by Ko and Ryou (2005) actually only includes the regions of coalescence and stretching as well as reflexive separation, defined with the Ashgriz and Poo (1990) boundary lines. The small region of bouncing indicated for very small We and large *B* in the utilised water-type collision map was not considered (see Figure 3 in Ko and Ryou 2005). The main contribution of their work was related to the development of a satellite formation model after separating collisions. With this hybrid model, Euler/Lagrange calculations of two interacting water sprays were conducted. The simulations showed that due to satellite droplet formation the Sauter mean diameter in the region of interacting sprays is considerably lower than in the case of single sprays.

Also, Mannannur and Reitz (2007) introduced a composite model for the droplet collision map using the boundary line for bouncing (Ethanol: Estrade et al. 1999), coalescence-stretching separation (water: Brazier-Smith et al. 1972) and reflexive separation (water: Ashgriz and Poo 1990). In the model for satellite droplet formation they however include viscous dissipation, which was neglected by Ko and Ryou (2005). The comparison of calculations with the proposed collision model showed a much better, though not perfect, agreement with measurements for impinging single droplet streams with different fuels, compared to those neglecting satellite droplet formation. A later study of the same group (Perini and Reitz 2016) used the same concept for defining the boundary lines of collision outcomes as a basis of the numerical prediction of single-pulse dodecane fuel sprays. However, they used the concept of the sphere-of-influence to search for parcel collision partners in order to relax the grid-size dependence of the collision detection procedure.

The impingement of two Diesel sprays was numerically computed by Kim et al. (2009) introducing some modifications to the classical O`Rourke (1981) collision detection model for insuring that the two statistically selected collision parcels are also moving towards each other and that the travel distance within one time step should be larger than their initial spatial separation (Nordin 2001). Besides not clearly describing how the possible collision partners are selected, also no fundamental validation of their model modifications was done, e.g. comparison with a fully deterministic collision detection model. For describing the droplet collision outcomes, a three-line boundary model was applied also accounting for satellite production during separative collisions. Misleadingly, again the boundary lines for water were applied for a Diesel spray (Kim et al. 2009). As described already, with the single-boundary

line model the coalescence rate is remarkably over-predicted compared to a three-line model including bouncing.

The effect of modified collision maps with increasing pressure (see Qian and Law 1997) was modelled by introducing a pressure coefficient in the Estrade et al. (1999) bouncing boundary line yielding a displacement to higher Weber numbers with increasing pressure (Zhang et al. 2016). Again, the grid-size-dependence of the spray penetration depth was shown without a further analysis why with finer meshes the collision rate increases and hence droplets become larger yielding higher spray penetration. The results for interacting sprays show the same trends mentioned above when comparing single-line and three-line boundary models.

Finally, the question is; which is the influence of the shape of the presumed collision map and the considered boundary lines on the calculated spray behaviour. Recent Euler/Lagrange calculations of Sommerfeld and Lain (2017) for a hollow cone water spray first of all showed that impact efficiency is essential to be accounted for and reduces the overall collision rate by 20 %. In these simulations a three-boundary line composite model (i.e. water-type collision map with bouncing, stretching and reflexive separation) was used. The observed collision outcomes were: coalescence 68%, bouncing 16%, stretching 16% and reflexive separation 1% when using the SS-C boundary after Ashgriz and Poo (1990). Naturally, the collision rates reduce alongside the spray where coalescence and bouncing occurs along the entire spray (length of the computational domain 1000 mm). Stretching was only observed until the middle region of the spray and reflexive separation just in the initial region, up to about 100 mm. Due to coalescence, of course, an increase of the averaged Sauter mean diameter along the spray was observed (i.e. from about 57 μm at injection to 65 μm at x = 600 mm). Now when using another SS-C boundary, for example according to Brazier-Smith et al. (1972) or Jiang et al. (1992), the coalescence probability will increase for large B (discussion see below in Figure 8) and the Sauter mean diameter grows much more rapidly along the spray. This reveals the importance and need of having appropriate boundary line models on droplet collision outcomes for refined spray simulations.

An analysis of the influence of the type of collision map used in spray computations was also conducted by Finotello et al. (2019) applying an LES (large eddy simulation)-Euler/Lagrange approach and the DSMC (direct simulation Monte Carlo) semi-stochastic collision model. The comparison of numerically obtained collision frequencies using collision maps for water compared to that for milk, showed the highest over-all collisions for water. This is caused by the special feature of the milk-type collision map showing no bouncing

independent of the solid content. This implies that most collisions result in coalescence reducing the droplet number density and hence collision frequency. When the solid content of the milk was increased (i.e. increasing viscosity) the SS-C boundary is moved upwards and to the right giving even more coalescence, further decreasing droplet number density and consequently reducing collision rates. Therefore, this work (Finotello et al. 2019) also demonstrates the importance of properly selecting the collision map according to the liquid at hand. In this study it was also revealed that even using an LES method for spray predictions, turbulent dispersion of the droplets by the unresolved sub-grid-scale turbulence needs to be modelled since turbulence remarkably increases droplet collision rate. Finally, it was also found (Finotello et al. 2019) that in the case of spray droplet size distributions, the collision probability for small size ratios (i.e. $\Delta < 0.5$) is considerably higher.

The present contribution highlights the importance of the presumed collision maps on the numerically calculated spray evolution and the resulting droplet size distributions. First, the fundamentals of the applied Euler/Lagrange approach with the involved models, especially the fully stochastic collision model, are described and the considered test case together with the applied different collision maps are introduced. In the results section, first the sensitivity of the fully stochastic collision model with regard to mesh size, parcel number and Lagrangian time step size is analysed. Then the influence of the assumed collision maps on the conditional collision numbers along the spray is critically assessed, followed by an evaluation of the predicted Sauter mean diameter along the spray and the resulting local droplet mass-based distributions. An important contribution is the evaluation of the existing droplet size ratios upon collision throughout the spray. Finally, the numerical predictions are compared with measurements and the conclusions from the research are presented.

2 Euler/Lagrange approach and test case definition

The numerical scheme adopted to simulate the dispersed two-phase flow developing in the spraying system is the fully coupled stationary and three-dimensional Euler/Lagrange approach (Laín et al. 2002). The fluid flow was calculated based on the Euler approach by solving the Reynolds-averaged conservation equations (mostly referred to as RANS equations) in connection with the standard k-ε turbulence model equations. The effect of the particle phase on the fluid flow was accounted for by appropriate source terms in the momentum equations as well as the conservation equations for turbulent kinetic energy and dissipation rate, i.e. referred to as full two-way coupling (Kohnen and Sommerfeld, 1997).

RANS calculation of fluid flow

The time-dependent three-dimensional conservation equations for an incompressible fluid may be written in the general form as:

$$\frac{\partial U_i}{\partial x_i} = 0 \tag{7}$$

$$\frac{\partial(\rho U_i)}{\partial t} + \frac{\partial\left(\rho U_j U_i\right)}{\partial x_j} = -\frac{\partial}{\partial x_i}\left(P + \frac{2}{3}\rho k\right) + \frac{\partial}{\partial x_j}\left[(\mu + \mu_T)\left(\frac{\partial U_i}{\partial x_j} + \frac{\partial U_j}{\partial x_i}\right)\right] + \rho g_i + S_{U_i p} \tag{8}$$

$$\frac{\partial(\rho k)}{\partial t} + \frac{\partial\left(\rho k U_j\right)}{\partial x_j} = \frac{\partial}{\partial x_j}\left[\left(\mu + \frac{\mu_T}{\sigma_k}\right)\frac{\partial k}{\partial x_j}\right] + \mathcal{P} - \rho\varepsilon + S_{kp} \tag{9}$$

$$\frac{\partial(\rho\varepsilon)}{\partial t} + \frac{\partial\left(\rho\varepsilon U_j\right)}{\partial x_j} = \frac{\partial}{\partial x_j}\left[\left(\mu + \frac{\mu_T}{\sigma_\varepsilon}\right)\frac{\partial \varepsilon}{\partial x_j}\right] + \frac{\varepsilon}{k}(C_{\varepsilon 1}\mathcal{P} - C_{\varepsilon 2}\rho\varepsilon) + S_{\varepsilon p} \tag{10}$$

Here, ρ is the gas density, μ its viscosity, U_i and P are the Reynolds-averaged velocity components and pressure, respectively. Eqn. (9) – (10) solve for the turbulent variables: the turbulent kinetic energy, k, and its dissipation rate, ε. Furthermore, μ_T is the turbulent viscosity, $\mathcal{P}$ is the trace of the production tensor which are written as:

$$\mu_T = \rho C_\mu \frac{k^2}{\varepsilon} \tag{11}$$

$$\mathcal{P} = -\rho\mathcal{R}_{ij}\frac{\partial U_i}{\partial x_j} \tag{12}$$

where $\mathcal{R}_{ij}$ is the Reynolds Stress tensor, closed in the $k - \varepsilon$ turbulence model as:

$$\rho\mathcal{R}_{ij} = \frac{2}{3}\rho k\delta_{ij} - \mu_T\left(\frac{\partial U_i}{\partial x_j} + \frac{\partial U_j}{\partial x_i}\right) \tag{13}$$

and δ_{ij} is the Kronecker delta. The model constants adopt the standard values given in Table 1.

C_μ	σ_k	σ_ε	$C_{\varepsilon 1}$	$C_{\varepsilon 2}$
0.09	1.0	1.3	1.44	1.92

Table 1: Constants for the $k - \varepsilon$ turbulence model.

The terms $S_{\phi p}$ in Eqn. (8) – (10) represent the additional source terms due to the phase interaction for the different variables $\phi = \{U_i, k, \varepsilon\}$ and they will be specified below.

Lagrangian droplet tracking

The simulation of the particle phase by the Lagrangian approach requires the solution of the equations of the motion for each computational particle along their path. This equation includes all interfacial and field forces the particle inertia, drag and gravity-buoyancy. The Basset history term, the added mass and the fluid inertia are negligible for the considered high ratios of droplet to gas density (in this work of $\mathcal{O}(10^3)$). Additionally, it is supposed that droplets do not rotate as a rigid body, so that also the rotational lift force may be neglected (Sommerfeld et al. 2008). Moreover, the shear-induced lift force is neglected here, as the droplets are rather small < 100µm and the shear gradients within the spray flow are not very strong as for example in a boundary layer (Sommerfeld et al. 2008). Under such approximations, the equations of motion for the droplets are given by:

$$\frac{dx_{di}}{dt} = u_{di} \tag{14}$$

$$m_d \frac{du_{di}}{dt} = \frac{3}{4}\frac{\rho}{d} m_d C_D (u_i - u_{di})|\vec{u} - \vec{u}_d| + m_d g_i \left(1 - \frac{\rho}{\rho_d}\right) \tag{15}$$

here, x_{di} are the droplet coordinates along their trajectories, u_{di} are its velocity components, $u_i = U_i + u'_i$ is the instantaneous velocity of the gas composed of mean value and instantaneous fluctuation, d is the droplet diameter and ρ_d the droplet material density. Moreover, $m_d = \pi \rho_d d^3/6$ is the droplet mass. The drag coefficient is obtained using the standard correlation (Schiller and Naumann, 1933):

$$C_D = \begin{cases} 24 Re_d^{-1}\left(1 + 0.15 Re_d^{0.687}\right) & Re_d \leq 1000 \\ 0.44 & Re_d > 1000 \end{cases} \tag{16}$$

being $Re_d = \rho d|\vec{u} - \vec{u}_d|/\mu$ the droplet Reynolds number. The instantaneous fluid velocity seen by the droplet is obtained by interpolating the fluid mean velocity from the neighbouring grid points to the particle position and adding a fluctuating component obtained from a single-step Langevin model (Lain and Sommerfeld, 2013).

The equations to calculate the particle motion are solved by integration of the differential equations (Eqn. 14 - 15). For sufficiently small time steps and assuming that the forces remain

constant during this time step, the new particle location and the linear velocities are calculated. The time step for the particle tracking, Δt_L, was chosen to be 50 % of the smallest of all local relevant time scales, such as the droplet relaxation time, the integral time scale of turbulence and the mean inter-particle collision time. Due to the applied series expansion in the derivation of the collision probability (Sommerfeld and Zivkovic 1992, Rüger et al. 2000), the local inter-particle collision time scale was additionally limited to $\Delta t_C < 0.05\,\tau_C$. In this way the numerical stability of the tracking algorithm is guaranteed (Göz et al 2004).

When a droplet hits the walls, it is assumed that it deposits and hence the parcel is removed from the computations. From an experimental point of view this assumption is also realistic, since the droplet liquid was water and the walls consisted of Plexiglass, consequently one has wetting conditions. For the purpose of demonstrating the effect of the droplet-wall boundary condition also computations with a specular refection of the droplets on the walls will be shown. Collisions among droplets are modelled by the fully stochastic approach of Sommerfeld (2001) which is described in detail below.

Influence of droplets on the carrier flow

After a converged solution of the fluid flow is obtained, a set of parcels (in the standard case 2,852,000 parcels) is tracked through the flow field until all leave the outlet boundary or stick on the wall. The source terms for the momentum equations resulting from the exchange between droplets and fluid are obtained on the basis of the Particle-Source-In-Cell (PSI Cell) concept (Crowe et al. 1977). Hence, the momentum exchange is calculated by averaging over all parcels traversing a given control volume during one Lagrangian calculation. Instead of summing up all individual fluid dynamic forces acting on the droplets, which may be quite cumbersome, the momentum exchange is calculated from the velocity change of the parcels when traversing the control volume. In this procedure however, the external forces have to be subtracted yielding the momentum source in the following form:

$$\overline{S_{U_i p}} = -\frac{1}{V_{cv}} \sum_k m_{dk} N_{dk} \sum_n \left\{ \left([u_{di}]_k^{n+1} - [u_{di}]_k^n \right) - g_i \left(1 - \frac{\rho}{\rho_d} \right) \Delta t_L \right\} \qquad (17)$$

where the sum over n indicates averaging along the particle trajectory (time averaging) and the sum over k is related to the number of computational particles passing the considered control volume with the volume V_{cv}. The mass of an individual droplet is m_{dk} and N_{dk} is the number of real droplets in one computational particle. Δt_L is the Lagrangian time step which is used in the solution of Eqn. (14) – (15). The source term in the conservation equation of the

turbulent kinetic energy, k, are expressed in the Reynolds averaging procedure as (Kohnen and Sommerfeld 1997):

$$S_{kp} = \sum_{i=1}^{3} \overline{u_i S_{U_i p}} - U_i \overline{S_{U_i p}} \tag{18}$$

$$S_{\varepsilon p} = C_{\varepsilon 3} \frac{\varepsilon}{k} S_{kp} \tag{19}$$

where the source term in the ε-equation has been modelled in the standard way with the parameter $C_{\varepsilon 3} = 1.8$. This value has been used in a wide range, i.e. $1.0 < C_{\varepsilon 3} < 1.9$, however, depends on the type of two-phase flow, as well as the particle concentration and particle size (Squires and Eaton 1993).

A converged solution of the coupled two-phase flow system is obtained by successive solution of the Eulerian and Lagrangian part, respectively. Initially, the flow field is calculated without particle phase source terms until a converged solution is achieved with the specified inlet conditions. Thereafter, a large number of parcels are injected and tracked through the flow field (2,852,000 computational particles in the present work) and the source terms are sampled for each control volume. In the first Lagrangian calculation droplet-droplet collisions are not considered, since the required cell-based droplet phase properties are not yet available. Hence, for each control volume the droplet concentration, the local droplet size distribution and the size-velocity correlations for the mean velocities and the rms values are sampled. These properties are updated each Lagrangian iteration in order to allow correct calculation of droplet-droplet collisions. Additional droplet phase properties and profiles may be sampled for each transverse cell when the computational particles cross a pre-defined location. From the second Eulerian calculation, the source terms of the dispersed phase are introduced using an under-relaxation procedure which provides the cumulative mean values of the source terms in each control volume (Kohnen et al. 1994). For the present calculations typically about *50* coupling iterations with an under-relaxation factor between *0.05* and *0.1* were necessary in order to yield convergence of the Euler-Lagrange coupling.

Stochastic Droplet Collision Model

The droplet collision model includes the following steps in order to determine the outcome of a binary collision. Since the parcel concept is used in order to include all real droplets produced by the spray, all droplets within the considered parcel behave in the same way and collide in the same way. These sub-processes in the applied fully stochastic collision model are (Sommerfeld 2017 b):

- Generation of a fictitious collision partner with size and mean velocities from the local droplet population (cell-based droplet properties were evaluated),
- Determination of the fluctuating velocity components of the fictitious parcel considering a possible correlation with those of the real parcel as a result of the interaction with the same turbulence structure,
- Transformation of the velocity components of the involved collision partners so that the larger droplet is stationary and the major axis of the collision cylinder is aligned with the relative velocity vector,
- Consideration of the impact efficiency and determination of the boundary droplet trajectory (lateral displacement Y_C) based on the results of Schuch and Löffler (1978),
- Stochastic determination of the impact location on the surface of the larger, collector droplet and determination of instantaneous collision Weber-number (Eq. (1)) and impact parameter *B* (Eq. (2)),
- Determination of the type of droplet collision occurring using the appropriate collision map $B = f(We)$,
- Evaluation of the droplet size (for coalescence only) and velocities after collision only for the real parcel and re-transformation into the laboratory frame of reference.

In this study, the fully stochastic collision model is applied where for each computational particle, or parcel, and during each Lagrangian time step a fictitious collision partner is created from the local population of droplets. The properties of the droplet population in each computational cell were statistically sampled during the previous coupling iteration for steady-state computations or during the previous Eulerian time step as described above. For the considered isothermal spray the required local properties are number concentration and size distribution of droplets, as well as the correlations between droplet size and mean velocities as well as rms values for each component. For obtaining the properties of the fictitious droplet, first a size is randomly drawn from the local cumulative size distribution. The next step is the determination of the instantaneous relative velocity between real and fictitious droplet. With the fictitious droplet size, the size-velocity correlations give the fictitious droplet mean velocity components. Naturally, for colliding droplets, which supposedly moved through the same turbulence structures before collision, their velocity fluctuation is not completely uncorrelated. Only a fully deterministic collision model would

yield the exact instantaneous relative velocity between colliding particles. In the fully stochastic collision model, a Langevin model is applied to create the fictitious droplet velocity fluctuating components *i* from that of the real droplet or parcel using a particle-pair velocity correlation function depending on the fictitious particle response time and the local integral time scale of turbulence, which is the Stokes number *St*. This correlation function was previously determined by comparing particle tracking simulations with results from large eddy simulations (LES) for homogeneous isotropic turbulence as described in Sommerfeld (2001). Based on the fundamental studies of Lain (2010) this correlation function was revised and the fictitious droplet fluctuating velocities are determined in the following way through a Langevin model:

$$u'_{fict,i} = R(\tau_P, T_L)\; u'_{real,i} + \sigma_i \sqrt{1 - R(\tau_P, T_L)^2}\; \xi_n \tag{20}$$

$$R(\tau_P, T_L) = R(St) = exp\left(\frac{0.019\; St^2}{1 + 0.044\; St^{1.725}}\right) \tag{21}$$

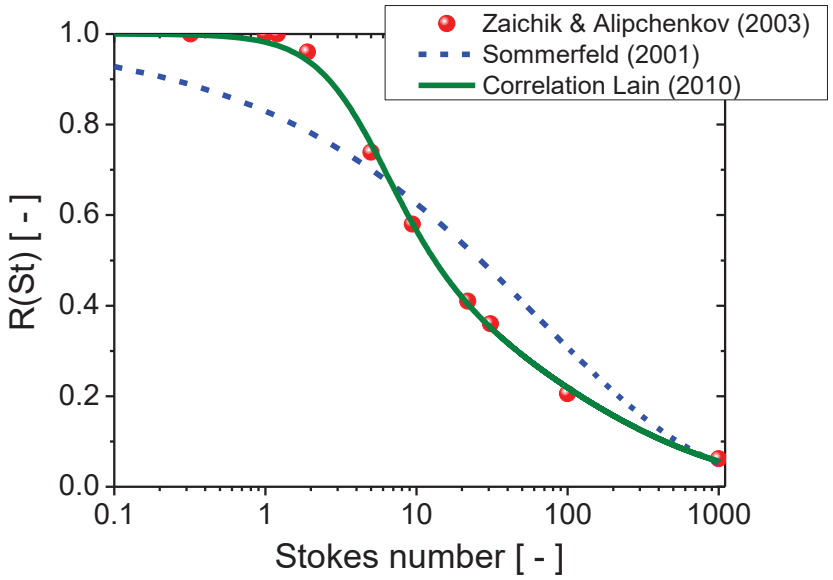

Figure 3: Particle pair velocity correlation function in dependence of particle Stokes number comparing different previously presented theories and correlations.

The correlation (21) was established by solving the Zaichik and Alipchenkov (2003) model for the correlation function of particle pair fluctuating velocities and fitting a three-parameter curve (Lain 2010). From Figure 3, it is obvious that such an expression is more appropriate than the two-parameter correlation proposed initially by Sommerfeld (2001).

Compared to just using the collision probability from kinetic theory, accounting for this velocity correlation of colliding droplets reduces drastically the collision frequency of

responsive droplets (Sommerfeld 2001). In sprays of course the produced smaller droplets have mostly such behaviour, so that neglecting this effect will again drastically influence in the predicted droplet size spectrum. In the spray calculations, the fictitious droplet might be the smaller or the larger droplet. Having now all properties of both droplets the collision probability based on kinetic theory of gases can be calculated:

$$P = \frac{\pi}{6} (d_S + d_L)^2 \, |\overrightarrow{u_S} - \overrightarrow{u_L}| \, n_d \, \Delta t_L \tag{22}$$

When a random number drawn from a constant probability (i.e. ξ_n: $[0,\ 1]$) becomes smaller than this probability, a collision takes place. In order to insure, that only binary collisions occur and since the probability of only one collision was derived from a series expansion, the Lagrangian tracking time step should be small enough not to exceed 10 – 20 % of the local inter-particle collision time (Zivkovic and Sommerfeld 1992).

An essential element which has to be integrated in the impact point determination is the impact efficiency which is relevant for a collision between small and large droplets (Ho and Sommerfeld 2002). In such a situation the smaller droplet might move around the larger one with the relative velocity field, which is a quite frequent phenomenon in sprays due to the wide droplet size spectrum normally existing. Effectively, impact efficiency results in a reduction of collision cross-section and hence collision rate (Sommerfeld and Lain 2017), since often larger droplets will capture smaller droplets due to the existence of high relative velocities (see Figure 4). This phenomenon may be described in a coordinate system where the larger collector droplet is stationary. Considering only inertial effects, the impact efficiency is then defined as the ratio of the circular cross-section from which the small droplets comes and just hits the larger droplet to the effective collector cross-section. Accounting also for the so-called blocking effect this cross-section diameter is the sum of the large and small droplet diameter (Figure 4). Hence, the impact efficiency follows as:

$$\eta = \left(\frac{2\, Y_C}{d_S + d_L}\right)^2 = \left(\frac{St_{rel}}{St_{rel} + a}\right)^b \tag{23}$$

In the work of Schuch and Löffler (1978) the impact efficiency for inertial effects was calculated in dependence of the relative Stokes number which is the small droplet Stokesian relaxation time to the time it needs to pass the collector droplet (Ho and Sommerfeld 2002) with the relative velocity:

$$St_{rel} = \frac{\tau_P}{T_{Pass}} = \frac{\rho_S \, d_S^2 \, u_{rel}}{18 \, \mu \, d_L} \tag{24}$$

here the d_S and d_L refer to the diameters of the small and large droplet, respectively, ρ_S is the small droplet density and u_{rel} is the instantaneous relative velocity. The impact efficiency (Eq. 23) was then related to the relative Stokes number using two parameters a and b, which depend on the collector droplet Reynolds number Re_c determined with the relative velocity (Schuch and Löffler 1978). This dependence is caused by the fact that with increasing collector Reynolds number the flow deviation is increasingly compressed towards the collector and so are the streamlines. The numerically obtained different values for the constants a and b are provided in Table 2. For that purpose, different numerical approaches were used (Schuch and Löffler 1978), such as boundary layer theory for small Re_c and potential theory for large Re_c. The results of the different correlations are given in Figure 5 together with own simulations which agree fairly well. These simulations were conducted solving the three-dimensional Navier-Stokes equations (i.e. without turbulence model) and conducting a Lagrangian point-particle tracking of many fine particles. Especially, at higher collector Reynolds numbers some differences are observed for small Stokes numbers (i.e. small particles) in Figure 5, since in the conducted computations boundary layer and wake of the collector are resolved, which is of course not possible by potential theory (Schuch and Löffler 1978). For a given relative Stokes number the increase in Reynolds number yields growing impact efficiency (Sommerfeld and Lain 2009) due the increasing small particle inertia as a result of the stronger flow deflection.

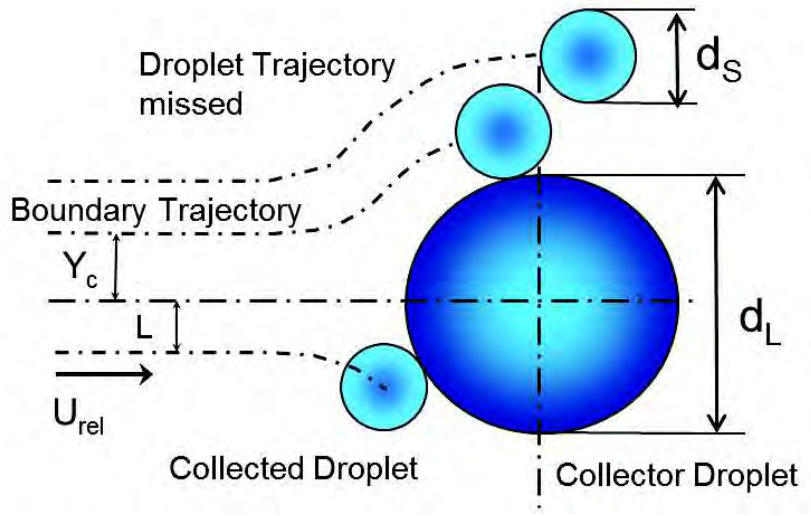

Figure 4: Illustration of inertial impact efficiency for the collision of a small droplet approaching a larger collector droplet with the relative velocity (shown in a transformed coordinate system where the collector is stationary and the relative velocity is aligned with the collision cylinder axis).

Eventually, a collision is only occurring if a randomly drawn lateral displacement L (see Sommerfeld 2001) is smaller than the value of Y_c. This instantaneous lateral displacement of the fine droplet from the axis of the collision cylinder as well as the angular position in the cross-section is determined by independent random processes (Sommerfeld 2001). Hence a collision occurs only if:

$$L \leq Y_C + 0.5\ D_S \tag{25}$$

Re_c	a	b
≥ 100	0.25	2.0
60 – 80	0.506	1.84
40	1.03	2.07
10 – 20	1.24	1.95
< 1	0.65	3.7

Table 2: Constants for the correlation proposed by Schuch and Löffler (1978) for the inertial impact efficiency (Eq. 23).

Strictly speaking, the above model for considering the inertial impact efficiency may be only applied to turbulent flows if the collision complex is much smaller than the smallest turbulent eddies, namely the Kolmogorov length scale, or the small droplets are quite inertial and hardly follow these small turbulent structures. Hence, here only inertial impacts are considered. Otherwise of course the impact efficiency is still very important, but the collision geometry is much more complex. In such a situation the trajectories of the small colliding droplets are affected by turbulent transport, so that even small droplets moving initially outside the collision cross-section might hit the collector due to turbulent diffusion. This regime is called turbulent diffusional impact. Thereby the impact efficiency will rise again when reducing the Stokes number below about *0.1* (Figure 5). This will happen in a similar way if the colliding droplets are very small so that their motion is affected by Brownian dispersion.

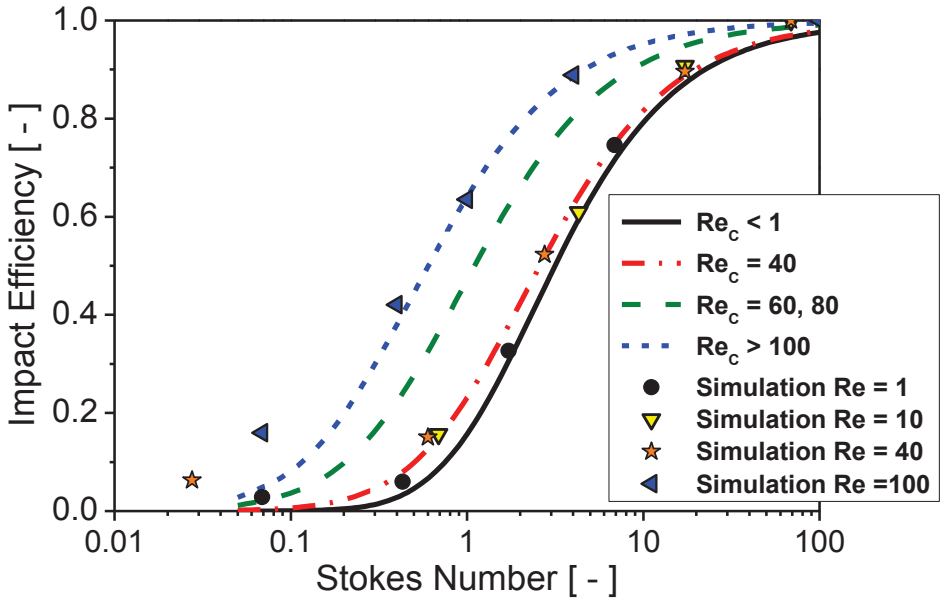

Figure 5: Inertia-based impact efficiency as a function of relative Stokes number, lines: correlations proposed by Schuch and Löffler (1978); symbols: numerical calculations (Sommerfeld and Lain 2009).

The next step in the droplet collision model is the determination of the collision outcome based on the collision maps $B = f(We)$ as it was described above (Figure 2) and the theoretically derived boundary lines, which will be presented in the test case description.

Finally, depending on the type of collision outcome, the properties and especially the velocities of the considered droplet have to be determined. The fictitious collision partner is not of interest anymore and the number of collisions calculated is identical to the number of droplets in the real parcel.

- If the outcome is bouncing, the parcels are reflected back with opposite normal velocity component by keeping the lateral component and thereby neglecting momentum los.
- In case of coalescence, the same approach used by Rüger et al. (2000) is applied: the new velocity of the new parcel is computed as the mass weighted velocity of the colliding droplets (R: real and F: fictitious droplet), the new diameter is given by the fact that the mass of the new droplet is the sum of the individual masses before collision, however, to comply with mass balance the new number of droplets in the coalesced parcel has to be reduced accordingly.

$$U_{R,i}^{'} = \frac{m_R\, U_{R,i} + m_F\, U_{F,i}}{m_R + m_F} \tag{26}$$

$$D_R^{'} = \left(D_R^3 + D_F^3\right)^{1/3}; \qquad N_R^{'} = N_R\, \frac{D_R^3}{D_R^3 + D_F^3} \tag{27}$$

- In case of stretching separation outcome, the parcels direction of motion is maintained and their velocities are reduced due to the dissipation generated by the interaction (O'Rourke, 1981).

$$U_{R,i}^{'} = \frac{m_R\ U_{R,i} + m_F\ U_{F,i} + m_F\left(U_{R,i} - U_{F,i}\right)\frac{B - B_{SS-C}}{1 - B_{SS-C}}}{m_R + m_F} \tag{28}$$

where B_{SS-C} is the normalised impact parameter obtained with the considered SS-C boundary line (e.g. Eq. (31)) at the Weber number of the collision and B is the actual impact parameter of the occurring collision.

- Finally, in case of reflexive separation, it is assumed that the collision partners conserve their sizes and are repelling each other but with reduced velocities accounting for the dissipation in the collision process (Tennison et al. 1998).

$$U_{R,i}^{'} = \frac{m_R\ U_{R,i} + m_F\ U_{F,i} \pm m_F\left(U_{R,i} - U_{F,i}\right)\sqrt{1 - \frac{We_C}{We}}}{m_R + m_F} \tag{29}$$

In the numerator ± indicates that the positive sign is used if the real parcel represents the small droplet and the negative sign is used if the droplet is the larger one. The dissipation term depends on the ratio between the critical Weber-number, We_C (see Figure 2) and the collision We-number and is consequently increasing with growing difference between the two.

Discretisation and numerical setup

The three-dimensional computational domain consists of a cylinder 1 m long and radius 0.2 m, resembling the experimental rig used in Rüger et al. (2000) as shown in Figure 6 left). It was discretized by a non-uniform structured numerical grid consisting of approximately 700,000 control volumes, which was sufficient to obtain a grid independent solution. The mesh was built as an O-grid divided in five blocks where the discretization of the central block, containing the cylinder symmetry axis, is much finer than the rest of surrounding blocks (Figure 6 right). This arrangement allows reproducing adequately the high mean velocity gradients developing in the region close to the nozzle and at the spray border.

The upper circular boundary of the domain was established as a velocity inlet and it was located at 25 mm downstream of the nozzle exit which was the first cross-section where simultaneous measurements of both phases were possible (i.e. the liquid sheet breakup was largely completed at this location). Measurements of the gas phase were of course only done for one line over the cross-section (i.e. from the centre to the wall) providing axial and radial mean velocities as well as the turbulent kinetic energy. These data were used to create the plane of gas inlet velocities for each control volume. For the determination of the dissipation

rate a length scale of $l_e = 12\ mm$ was used. The lower circular cross-section was specified as outlet boundary condition (i.e. zero gradient for all properties) and it was located 1000 mm below the inlet cross-section. The lateral cylinder wall was set as a non-slip condition for the gas phase using standard wall functions. For the droplets, it was defined as an absorbing wall, i.e. as soon as a droplet touches the wall it is deposited and removed from the computation.

For generating the droplet injection conditions at the inlet pane ($z = 25\ mm$) results from PDA (phase Doppler anemometry) measurements were available. Again, these measurements were done along a single line over the radial range $0 < r < 30\ mm$ in distances of at least one millimetre. These data include the local droplet mass flux and the local droplet size distributions, as well as the size-velocity correlations for axial and radial mean velocities and the associated rms-values. The tangential (or lateral) velocity component for the droplets was not measured but may be assumed to be close to zero (hollow cone spray nozzle without swirl) and the rms-value should be almost identical to the radial component. Naturally, in the droplet or parcel injection procedure, the injection location was randomly selected over the entire inlet cross-section (i.e. diameter of 60 mm), however weighted according to the droplet mass flux.

The injection process for each parcel can be summarized as follows: first, a size was drawn from the local cumulative distribution function by a random process (the droplet size and the local mass flux determine the number of real droplets within a parcel); then, the size-velocity correlations provide the droplet mean velocity components; moreover, from the correlation between the size and rms-values the standard deviations for each velocity component are obtained. Hence, the instantaneous fluctuating velocity components were drawn from normal distribution functions with these rms-values.

The droplet parcels were continuously injected at the inlet and simultaneously tracked through the beforehand calculated stationary flow field (previous Eulerian computation) until all 2,852,000 parcels also have left though the outlet. As described above, during this time for each control volume the droplet properties and source terms were sampled. Profiles of all velocity components for the gas phase and the relevant droplet phase properties (i.e. droplet mean number diameter, droplet concentration and droplet velocity components) were evaluated at the measurement locations 25, 50, 100 and 200 mm.

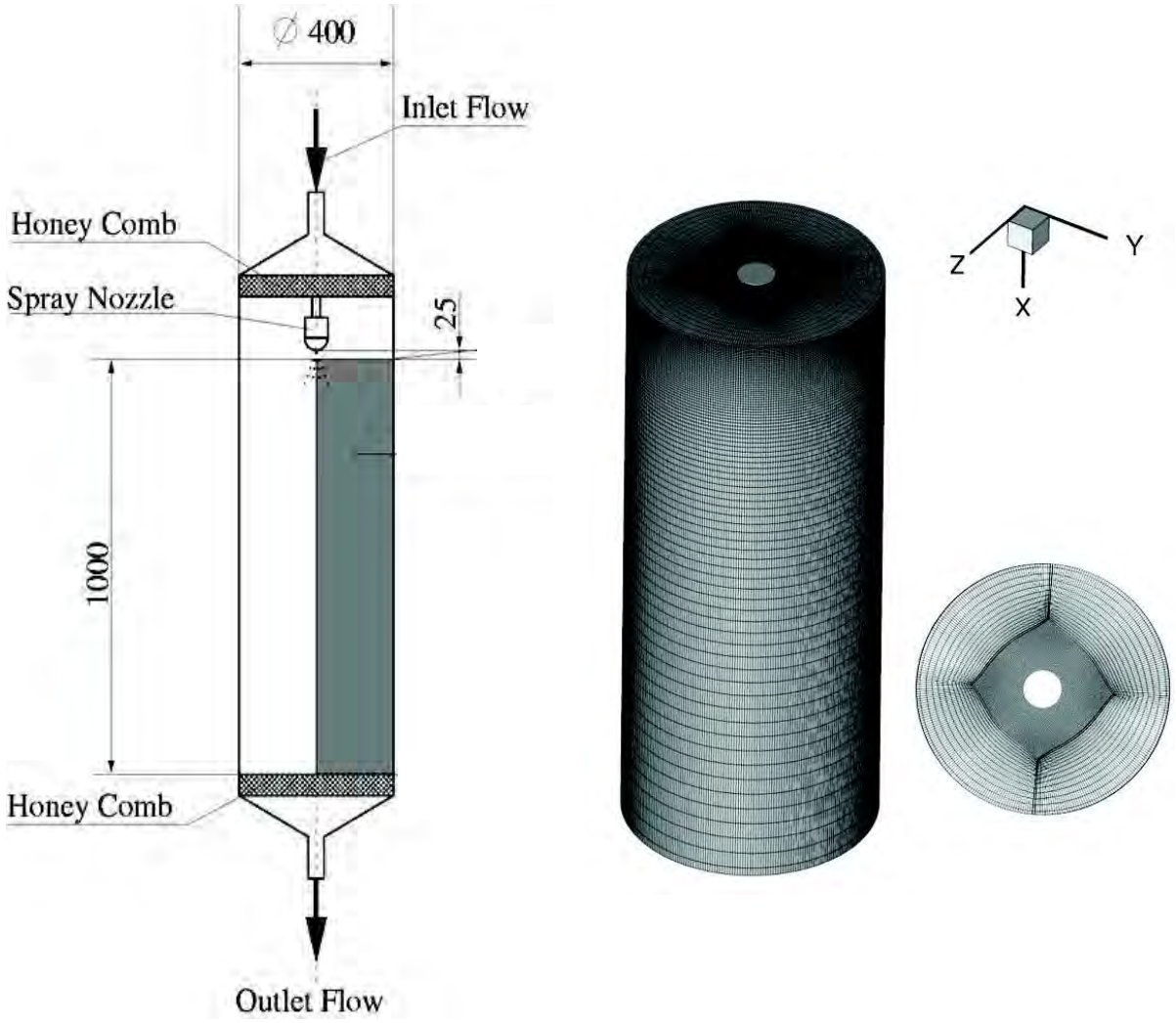

Figure 6: Configuration of the spray facility with inlet and outlet section as well as the nozzle arrangement as realised in the experiments, test section diameter 400 mm (left), numerical grid of the entire computational domain (right).

Definition of test cases

The main objective for the numerical simulations of the spray system described above was to analyse the influence of the beforehand defined collision map on the predicted spray characteristics, mainly the size or size distribution of the eventually produced droplets. This is a major goal for many technically realised spraying systems. The considered hollow cone water spray measured in detail by Rüger et al. (2000) is the validation case. Hence, the basic configuration of the collision map describing individual collision outcomes was that for water (Qian and Law 1997; Foissac et al. 2010; Kuschel and Sommerfeld 2013) as shown in Figure 7 a) with the lower boundary for bouncing, the boundary between stretching separation and coalescence (SS-C) and that between reflexive separation and coalescence (RS-C).

This collision map for water is a quite special case as bouncing is only observed for large impact parameters B (in the following indicated as water-type). The lower bouncing boundary is described by the well-known Estrade et al. (1999) correlation given below (Eq. (30)). The separation line between stretching separation and coalescence (SS-C) seems to be slightly better described by the Ashgriz and Poo (1990) boundary given in Eq. (32) compared to the Brazier-Smith et al. (1973) correlation given by Eq. (31) for the region above the bouncing boundary (see Figure 7a)). However, when considering the behaviour with decreasing size ratio Δ (Sommerfeld and Pasternak 2019), the Brazier-Smith et al. (1973) correlation (Eq. (31)) is superior. As mentioned above, many numerical computations have been performed with just a single boundary line between coalescence and grazing, mostly using the Brazier-Smith et al. (1972) equation (e.g. in O´Rourke 1981). Grazing includes bouncing and stretching separation. This approach however completely neglects the occurrence of reflexive separation being observed for small B and larger We. In this study, the boundary line RS-C is determined with the mostly applied Ashgriz and Poo (1990) correlation specified in Eq. (33).

When the viscosity of the liquid slightly increases and the surface tension is decreased to about half of that for water, bouncing is also observed for small We down to B = 0 as illustrated in Figure 7 b) for hexanol alcohol (Sommerfeld and Kuschel 2016). This behaviour is also observed for different hydrocarbon droplets in air at atmospheric pressure (Jiang et al. 1992) as well as tetradecane at different ambient pressures and for different environmental gases (Qian and Law 1997).

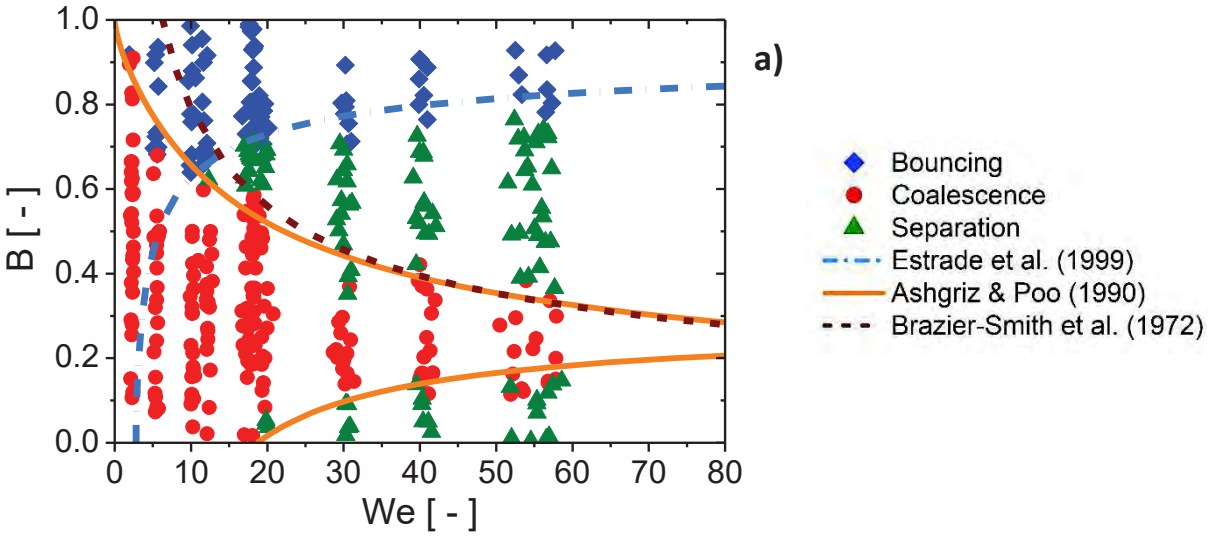

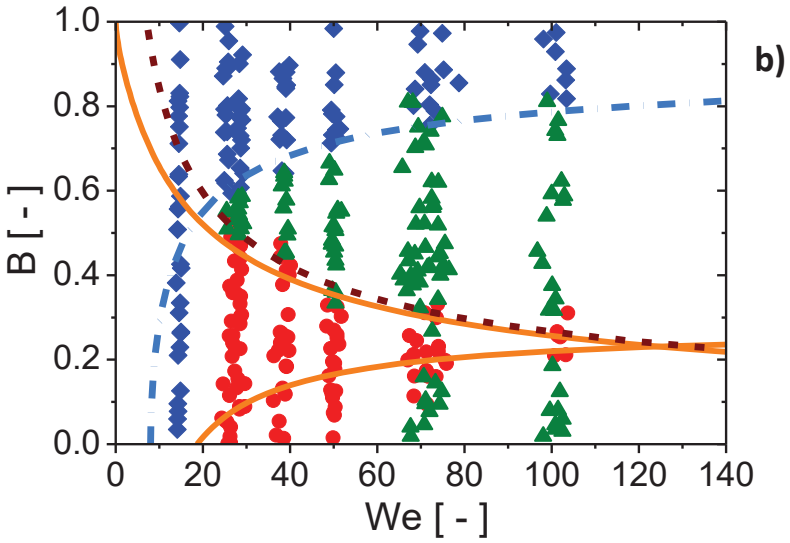

Figure 7: Collision maps experimentally obtained for identical droplets and two different liquids with theoretical boundary lines for lower bouncing by Estrade et al. (1999) Eq. (30), stretching separation-coalescence (SS-C) by Brazier-Smith et al. (1973) Eq. (31) and Ashgriz and Poo (1990) Eq. (32) as well as reflexive separation-coalescence (RS-C) by Ashgriz and Poo (1990) Eq. (33); **a)** water with Estrade shape factor $\Psi = 3.351$ (Kuschel and Sommerfeld 2013), **b)** hexanol alcohol with Estrade shape factor $\Psi = 3.8$ (Sommerfeld and Kuschel 2016).

Consequently, a series of numerical computations were conducted considering three boundary lines using available correlations as already mentioned in Figure 7, namely:

- The lower boundary of bouncing presented by Estrade et al. (1999) with shape factor $\Psi = 3.351$:

$$We = \frac{\Delta\left(1+\Delta^2\right)\left(4\,\Psi-12\right)}{\chi\,(\cos(\arcsin B))^2} \tag{30}$$

$$\chi = 1 - 0.25\,(2-\tau)^2(1+\tau) \qquad if: \tau > 1$$

$$\chi = 0.25\,\tau^2\,(3-\tau) \qquad if: \tau \leq 1$$

$$\tau = (1-B)\,(1-\Delta)$$

- The boundary between stretching separation and coalescence (SS-C) by Brazier-Smith et al. (1972), abbreviated by B-S below:

$$We = \frac{4.8}{B^2}\left(\left(\frac{1}{\Delta}\right)^3 - 2.4\left(\frac{1}{\Delta}\right)^2 + 2.7\left(\frac{1}{\Delta}\right)\right) \tag{31}$$

$$B = \frac{2.191}{We^{1/2}}\left(\left(\frac{1}{\Delta}\right)^3 - 2.4\left(\frac{1}{\Delta}\right)^2 + 2.7\left(\frac{1}{\Delta}\right)\right)^{1/2}$$

- Alternatively, the SS-C boundary by Ashgriz and Poo (1990), abbreviated with A&P below:

$$We = \frac{4\,(1-\Delta^3)^2\,\{3\,(1+\Delta)\,(1-B)\,(\Delta^3\,\phi_S+\phi_L)\}^{1/2}}{\Delta^2\,\{(1+\Delta^3)-(1-B^2)\,(\phi_S+\Delta^3\,\phi_L)\}} \tag{32}$$

$$\varphi_S = \begin{cases} 1-\dfrac{1}{4\,\Delta^3}(2\,\Delta-\tau)^2(\Delta+\tau) & for\ \square > 0.5d_S \\ \dfrac{\tau^2}{4\,\Delta^3}(3\,\Delta-\tau) & for\ \square < 0.5d_S \end{cases}$$

$$\varphi_L = \begin{cases} 1-\dfrac{1}{4}(2-\tau)^2(1+\tau) & for\ \square > 0.5d_L \\ \dfrac{\tau^2}{4}(3-\tau) & for\ \square < 0.5d_L \end{cases}$$

$$\square = \frac{1}{2}(d_L+d_S)(1-B); \qquad \tau = (1-B)\ (1+\Delta)$$

- And the reflexive separation-Coalescence boundary (RS-C) presented by Ashgriz and Poo (1990):

$$We = 3\left[7\,(1+\Delta^3)^{2/3}-4(1+\Delta^2)\right]\frac{\Delta\,(1+\Delta^3)^2}{\Delta^6\,\eta_S+\eta_L} \tag{33}$$

$$\eta_S = 2\,(1-\xi)^2\,(1-\xi^2)^{1/2}-1$$

$$\eta_L = 2\,(\Delta-\xi)^2\,(\Delta^2-\xi^2)^{1/2}-\Delta^3$$

$$\xi = (1/2)\ B\ (1+\Delta)$$

All these boundary lines, mostly based on energy balances, include the droplet size ratio as an additional parameter which in this study is either fixed to a value of $\Delta = 1$ or allowed to vary according to the size ratio at hand for the detected collision. The test cases considered in this study are summarised in Table 3. If the three-boundary line model is considered the bouncing boundary is always the same as given by Eq. 30 and also the same curve is used for the RS-C boundary (Eq. 33). Moreover, Table 3 includes the resulting droplet collision numbers, within the entire computational domain, in total and for the different scenarios of the outcomes, which will be discussed below. Please note that all these numbers are real droplet collisions and not parcel collision numbers. Actually, in average one parcel represents about 3 real droplets whereby for example in Case4 one droplet experiences in average only about 2 collisions in the entire computational domain.

In addition, for each case, the cross-sectional averages of the droplet collision numbers for all outcome types were determined along the spray. Velocity profiles for the spray droplets at the

cross-sections specified above are evaluated and compared to the available experimental data. In order to demonstrate the effect of droplet collisions for the different model assumptions, also droplet size distributions were sampled at distinct locations within the spray and compared to available measurement results. In order to assess the results obtained with the different collision maps, cross-sectional averages of the droplet Sauter mean diameter are plotted along the spray. Additionally, statistics on the droplet size ratios at the instant of a collisions were extracted from the simulations. This is a very important information which allows to emphasise needs in additional measurements and model developments. From the simulations such PDFs (probability density functions) were evaluated for different cross-sections in the spray and also conditionally sampled for the different collision outcomes.

Case	SS-C Boundary	Impact Efficiency	Delta	Type of collision map	Total Collisions
Case 0	----------	----------	----------	No droplet collisions considered	----------
Case 1a	A&P	no	1	water-type collision map	14,660,163
Case 1b	B-S	no	1	water-type collision map	14,496,176
Case 1c	B-S	no	1	water-type; single boundary	19,356,063
Case 2a	A&P	yes	1	water-type collision map	11,905,523
Case 2b	B-S	yes	1	water-type collision map	11,769,630
Case 2c	B-S	yes	1	water-type; single boundary	15,869,083
Case 3	A&P	yes	variable	water-type collision map	13,219,259
Case 4	B-S	yes	variable	water-type collision map	15,506,068
Case 5	B-S	yes	variable	bouncing to B=0	13,256,107
Case 6	B-S	yes	variable	bouncing to B=0; We +20	14,085,238

Case	Bouncing	[%]	Coalescence	[%]	Stretching	[%]	Reflexive	[%]
Case 0								
Case 1a	4,332,110	29.55	7,139,269	48.70	3,000,229	20.47	188,555	1.29
Case 1b	3,195,400	22.04	8,151,410	56.23	2,961,680	20.43	187,682	1.29
Case 1c	----------	---------	9,650,900	49.86	9,705,163	50.14	----------	---------
Case 2a	3,392,151	28.49	5,241,318	44.02	3,077,978	25.85	194,076	1.63
Case 2b	2,828,320	24.03	5,736,310	48.74	3,012,580	25.60	192,408	1.63
Case 2c	----------	---------	6,880,920	43.36	8,988,163	56.64	----------	---------
Case 3	2,074,007	15.69	9,005,929	68.13	2,121,665	16.05	17,658	0.13
Case 4	448,121	2.89	14,617,228	94.27	431,918	2.79	8,801	0.06
Case 5	6,069,098	45.78	6,749,953	50.92	428,303	3.23	8,753	0.07
Case 6	11,039,401	78.38	2,920,882	20.74	121,805	0.86	3,152	0.02

Table 3: Summary of the considered test cases for the comparison of the different droplet collision outcome models (collision maps $B = F\ (We)$ as summarised in Figure 8) together

with the obtained conditional collision numbers and their percentage from the total number of collisions.

The collision maps of all cases considered (Table 3) are summarised in Figure 8 for convenience. As mentioned above, the bouncing and RS-C boundary are for all cases were kept identical. The emphasis is on the influence of different boundary lines between stretching separation and coalescence (SS-C). The comparison of the resulting collision maps with the boundary lines for SS-C using the A&P and the B-S correlation are presented in Figure 8 a) used for the Cases 1a and 1b as well as for 2a and 2b, for both assuming $\Delta = 1$ no matter which size ratio is at hand in the collisions of the computations. It is clear that using the B-S boundary yields a reduction in the occurrence of bouncing and an enhancement of coalescence comparted to the A&P boundary. The Cases 3 and 4 consider a variable size ratio for the A&P as well as B-S boundary line which is illustrated in Figures 8 b) and c) by adding the dashed line for a size ratio of $\Delta = 0.5$. It should be noted, that with decreasing size ratio the bouncing boundary is shifted upwards and the RS-C boundary moves to the right. Regarding the SS-C boundary A&P predicts a turning of this line around the point $We = 0$ and $B = 1$ with decreasing size ratio, whereas the B-S curve yields a shift to the right-hand side. From experimental observations (e.g. Estrade et al. 1999) it is clear that the such a shift obtained with the B-S model is much more realistic than a turning predicted by A&P. Unfortunately, there are no experiments available on collisions of water droplets with different size ratio. As demonstrated in Figure 8 a) the B-S boundary for $\Delta = 1$ results in a small increase of coalescence and a decrease of bouncing compared to the A&P boundary when considering water-type collision maps. Hence, although the A&S model is slightly better in demarking the bouncing region for water as shown in Figure 7 a) it completely fails to correctly describe the boundary line change with decreasing size ratio. Consequently, the mostly used B-S boundary line for SS-C is to be preferred. With decreasing size ratio (here only $\Delta = 0.5$ is shown) the region of coalescence is enlarged much stronger when using the B-S instead of the A&P boundary (compare Figures 8 b) and c)). Therefore, it is expected that with the SS-C boundary according to B-S much larger droplets are produced by the spray.

For the Case 5 it is now assumed that the bouncing boundary goes down to $B = 0$, mimicking a higher viscous liquid (compare Figures 7 a) and b)) as illustrated in Figure 8 d) only for a size ratio of $\Delta = 1$. The open cycles indicate the bouncing boundary for the water-type collision map and corresponds to Case 4 also for $\Delta = 1$ only. The final collision map considered in the present simulation studies imposes a shift of the boundary curves by a value of 20 for the We number in order to mimic a much higher viscosity of the droplet liquid

(Kuschel and Sommerfeld 2013). For the SS-C boundary again the B-S correlation was used (see Figure 8 e)). Expectedly, such a collision map will favour more bouncing collisions, whereas the extent of the coalescence region remains almost unchanged.

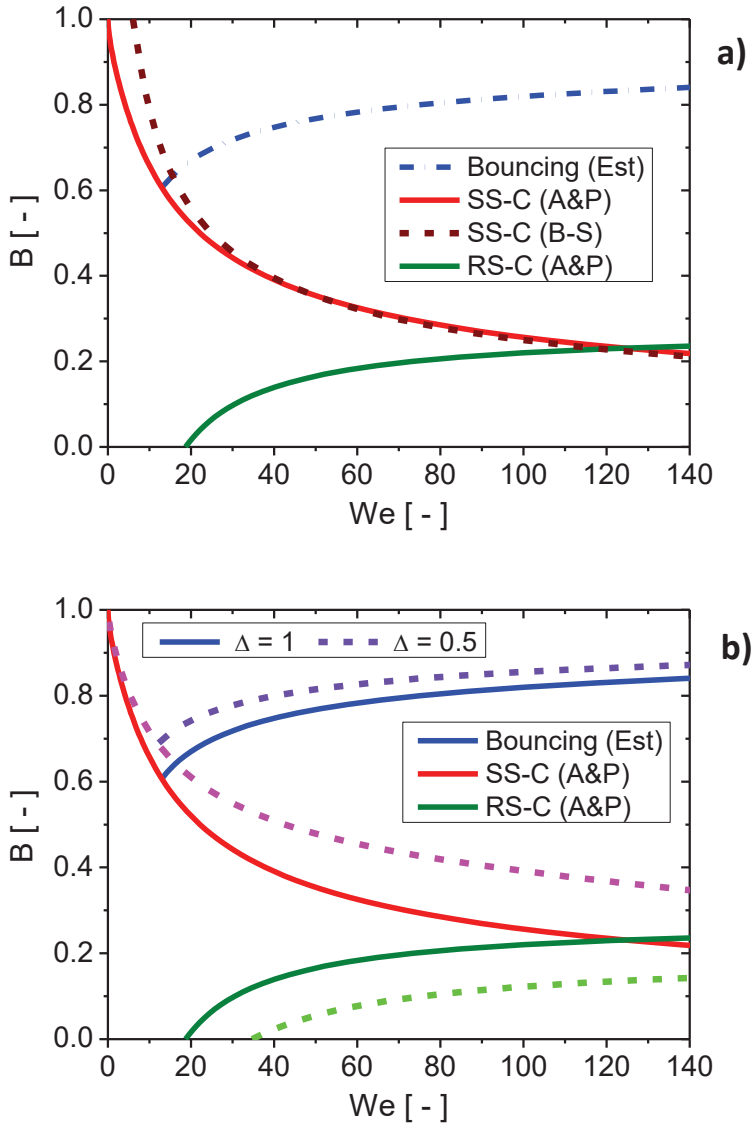

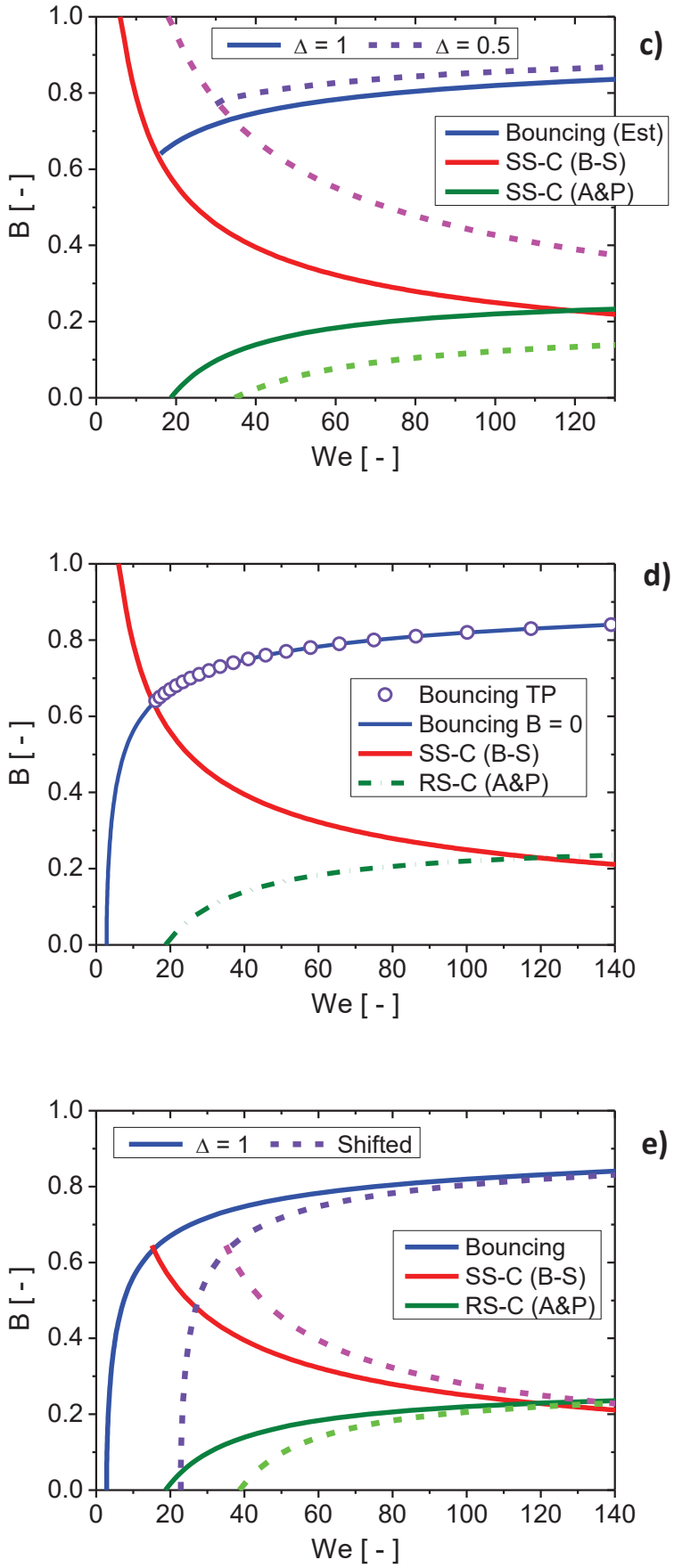

Figure 8: Summary of the different collision maps considered in the numerical computation of the spray as summarised in Table 2; boundary lines: bouncing by Estrade et al. (1999) Eq.

(30), SS-C by B-S: Brasier-Smith et al. (1972) Eq. (31), SS-C by A&P: Ashgriz and Poo (1990) Eq. (32) as well as RS-C by A&P: Ashgriz and Poo (1990) Eq. (33); **a)** relevant for Cases 1a, 1b, 2a and 2b with $\Delta = 1$ and bouncing ending at triple point (TP); **b)** relevant for Case 3, SS-C by A&P with full lines for $\Delta = 1$ and dashed lines for $\Delta = 0.5$; **c)** relevant for Case 4, SS-C by B-S with full lines for $\Delta = 1$ and dashed lines for $\Delta = 0.5$; **d)** relevant for Case 4 and 5, SS-C by B-S for $\Delta = 1$ with two options for bouncing-one: ending at triple point (Case 4); -two: ending at B=0; **e)** relevant for Case 6 (dashed lines) the boundary lines for Case 5 (closed lines) are shifted by We = 20 to the right (all boundary lines shown only for $\Delta = 1$.

4 Results and Discussion

In this section the obtained numerical results will be discussed on different levels. First the conditional droplet collision numbers along the spray according to their outcomes (i.e. bouncing, coalescence, stretching and reflexive separation) will be analysed for different presumed droplet collision maps. This allows conclusions with regard of the sensitivity of the predicted droplet sizes in a spray on the assumed collision maps. This issue will be highlighted by considering the droplet Sauter mean diameter along the spray. Then the predicted spray properties including droplet phase velocities will be compared with experiments accentuating the effect of the assumed droplet collision maps. Finally, also predicted local droplet size distributions will be compared.

Reliability of the fully stochastic droplet collision model

A review on the concepts of droplet collision detection and modelling was provided by Sommerfeld and Pasternak (2019), distinguishing between deterministic, deterministic-stochastic and fully stochastic collision detection, and by Pischke et al (2015) analysing hybrid droplet collision detection models. The fully stochastic droplet collision detection model applied in this study is known to be less sensitive to the issues discussed by Pischke et al. (2015) and especially the grid dependence of the obtained collision rates. For that purpose, spray simulations based on Case 4 (i.e. SS-C boundary by B-S) were conducted also with different limitations of the Lagrangian time step, a lower number of tracked parcels and a finer numerical grid. It should be noted, that in this study a stationary spray is considered only. In order to ensure a relative error of less than 2.5% due to the truncation of the series expansion of the collision probability P, the particle tracking time step should be limited to $\Delta t_C < 0.05\,\tau_C$ which was done in the standard computations presented in the following. For Case 4 now two additional runs were conducted with limiters of 0.1 and 0.2 yielding of course larger values for the total collision number in the spray presented in Table 3. This increase was 5.45% for a limiter of 0.1 and 11.96% when selecting a larger limiter of 0.2. A finer numerical grid with 1.0 million cells showed no large differences in the predicted flow field

of the spray for both gas and droplets. Due to the poorer statistics for the droplet phase in the case of a finer numerical grid, also the statistics of the cell-based droplet properties, needed for the collision model, is affected. This resulted in slightly lower total collision numbers of only 1.54%. Finally, also computations with much lower parcel numbers were conducted, again of course giving a poorer statistic for the cell-based droplet properties. In the standard case about 2.5 million parcels were tracked and now also simulations with 50% and 25% of this parcel number were done. The obtained total collision rates now increased by only 0.8% and 1.9% for these much lower parcel numbers. Hence, it may be concluded, that the applied fully stochastic collision model is very efficient, robust and reliable.

Droplet collision rates for different cases

The reference Case 0 without droplet collisions will be used only for comparing the velocity profiles along the spray and some local droplet size distributions. Expectedly, most of the droplet collisions occur just downstream of the numerical injection location (i.e. at $z = 25$ *mm*) due to the high droplet concentration and relative velocities, especially between small and large droplets. When the spray is spreading radially and the droplet velocity decays, also the collision rate drastically decreases and becomes very low from about 1000 mm downstream of the injection.

First the importance of the impact efficiency (IE) for numerical computations of spraying systems shall be emphasised. For that purpose, the water-type collision map with three boundary lines and with $\Delta = 1$ for clarity is considered. Hence, the cases 1a and 2a (A&P) as well as 1b and 2b (B-S) are compared. A clear picture is obtained by showing a bar chart for the collision numbers in the considered outcomes, comparing simulations without and with impact efficiency. In Figure 9 the result obtained with the A&P boundary line SS-C is shown. Neglecting this important physical effect, yields as to be expected, a drastic reduction of the collision numbers for bouncing and coalescence, whereas stretching and reflexive separation numbers slightly increase. This implies that neglecting impact efficiency results in an overprediction of the total collision number by 23 % in the case of using the A&P boundary for SS-C (i.e. compare Cases 1a and 2a). It should however be noted, that collisions affected by IE mainly concern smaller droplets that do not hit the collector, whereby eventually the Sauter mean diameter is not strongly affected, as will be discussed below. For the B-S boundary line model the total collision rates without and with IE (compare Case 1b and 2b) are about the same as from the A&P results, as given in Table 3. However, the number of coalescence outcomes is higher and bouncing slightly lower for the B-S compared to the A&P model as one would expect from Figure 8 a). It is also noticed that the most droplet collisions

occur with the outcome coalescence followed by bouncing. The percentage of the different collision outcomes in terms of the total collision number for the Cases 1a and 2a can be obtained from Table 3.

Now the number of droplet collisions along the spray is analysed according to the collision outcomes summarised in Figure 8. As shown in Figure 10 for the A&P case (see Figure 8 a)) the consideration of the impact efficiency reduces the collision rate. Especially as impact efficiency becomes more relevant for large B (see Figure 4), the bouncing number is remarkably reduced, but also coalescence is diminished as there is a small region with large B (see Figure 8 a)). Stretching and reflexive separation are hardly affected (Figure 10), only at a farther distance from the injection, where the collision number is anyway below about 100. A very similar behaviour is observed for the B-S boundary line between SS-C (not shown here). Consequently, the consideration of IE reduces coalescence whereby also the predicted droplet size produced by the spray will be overestimated when not accounting for IE. With respect to the final Sauter mean diameter this effect is small for the present spray as the droplets not colliding or coalescing also are expected to be small. The difference in the Sauter mean diameter is actually only about 1%.

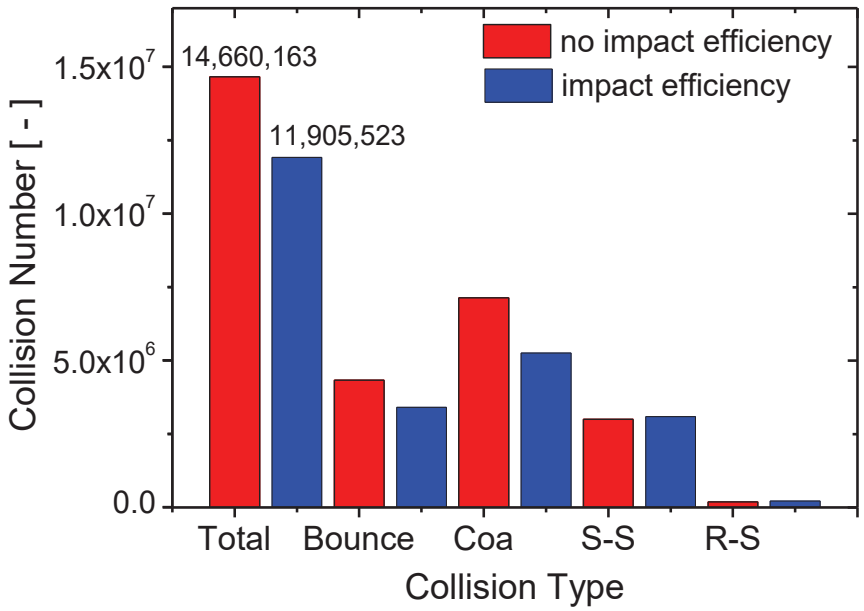

Figure 9: Number of droplet collisions in total and for the different collision outcomes without and with IE (impact efficiency), comparing Case 1a and 2a (SS-C boundary by A&P)

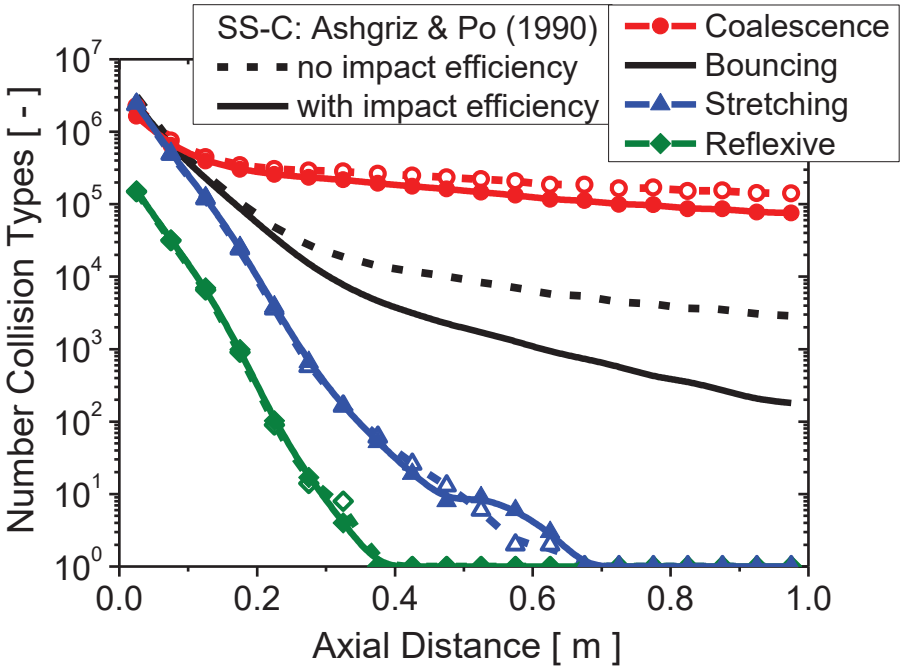

Figure 10: Collision numbers along the spray for the different collision outcomes, comparing without and with IE based on the SS-C boundary by A&P for $\Delta = 1$ (i.e. Case 1a and 2a).

From Figure 8 a) one would assume that there is not a huge difference between the SS-C models of A&P and B-S applied to a spray simulation. However, as many droplet collisions occur in the region of lower *We* in the collision map, at least for the spray considered here, there will be a remarkable difference in the conditional collision numbers. For illustrating the occurrence of the droplet collisions in the B-We space, a collision density plot is presented in Figure 11a) for the B-S boundary with IE and $\Delta = 1$ (Case 2b). Using the same boundary lines, however, with consideration of a variable Δ (Case 4) the collision density plot is very similar except for the region of large *B* and small *We* due to the shifting of the boundary line when Δ is reduced (Figure 11b). From the collision density plots, it is obvious that many collisions are observed for $We < 20$ over the entire *B*-range except for a small region below $B \approx 0.2$ and $0 < We < 20$. The number of collisions in the triangular region below a dividing line (i.e. We:B; 0:0; 100:1.0) is quite low, namely below about 100, which also implies that reflexive separation is rather low. Above this line the collision number is at least one order of magnitude higher, indicating that at larger *We* the occurrence of collisions with larger *B* is more likely to happen.

The resulting collision numbers along the spray for both the A&P (Case 2a) and the B-S (Case 2b) model, both with IE, are compared in Figure 12. Expectedly, with the B-S model the number of bouncing collisions is remarkably reduced mainly further downstream the nozzle, i.e. $z > 0.1$ m where the relative velocity and hence the Weber number is smaller.

Correspondingly, coalescence is increased in the initial spray region by about the same number (see Table 3). Please note that the vertical axis of Figure 12 is logarithmic. For the B-S model also a small reduction of collision numbers is observed for separation but father downstream which is due to the modification of the droplet size spectrum taking place in the initial spray region.

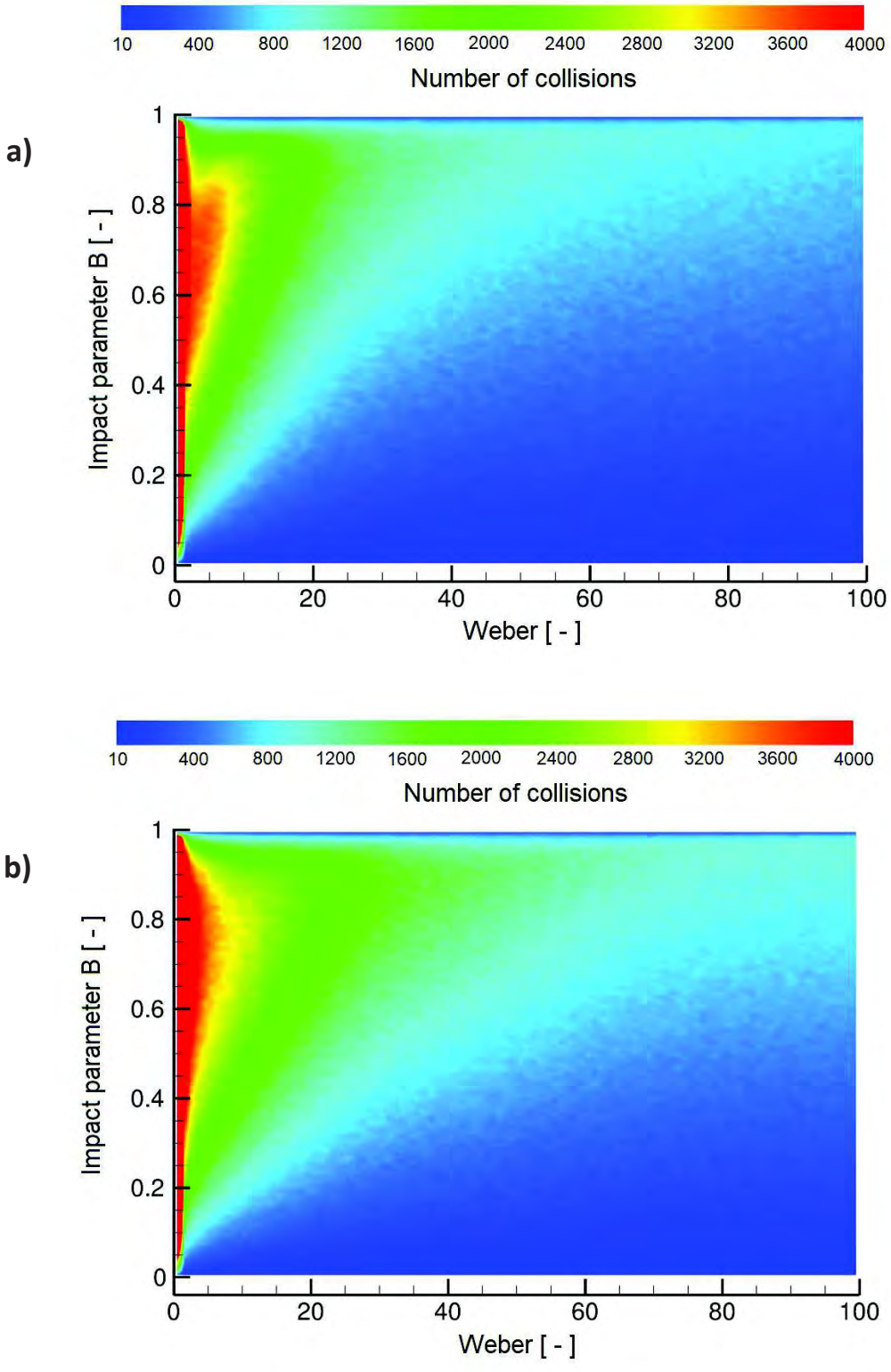

Figure 11: Collision density plot (i.e. B = f(We)) obtained for the entire spray with boundary lines for bouncing by Estrade et al. (1999), reflexive separation (RS-C) by Ashgriz and Poo (1990) and the SS-C boundary by B-S with IE and **a)** $\Delta = 1$ (i.e. Case 2b); **b)** with variable Δ (Case 4).

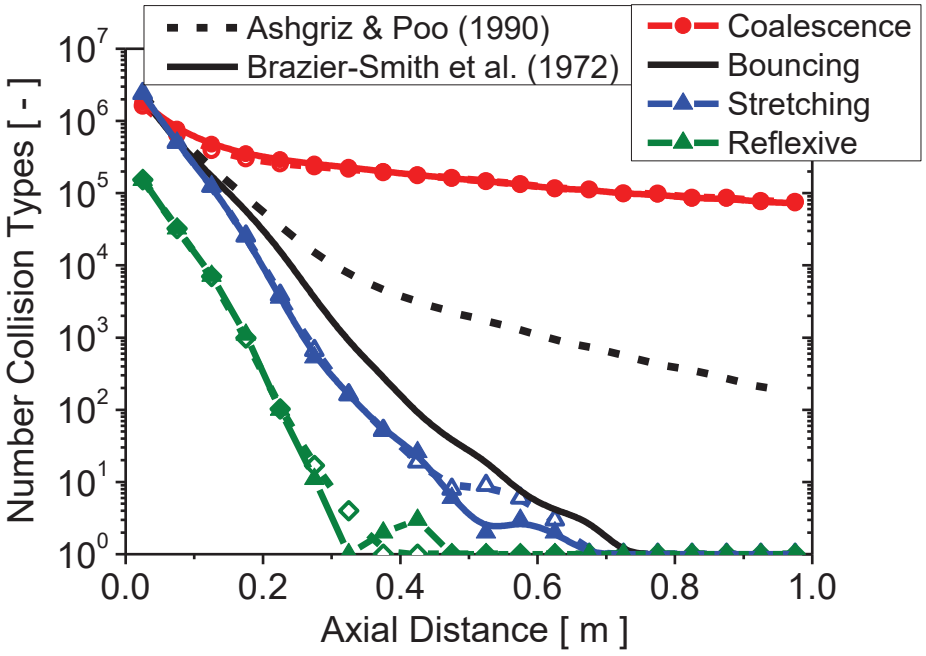

Figure 12: Collision numbers along the spray for the different collision outcomes, with IE and $\Delta = 1$, comparing the SS-C boundary by A&P and B-S (i.e. Case 2a and 2b).

As emphasised previously, many numerical computations of spray systems, including combusting sprays, are conducted with single-line boundary collision maps, often using the B-S model, which is also done here for comparison. Thereby, of course the occurrence of reflexive separation is neglected. Moreover, it is not possible to model any satellite formation upon stretching separation. Hence, a single-line model will of course increase the region of coalescence and the resulting collision numbers as shown in Figure 13 where the 1-line boundary (Case 2c) produces more coalescence and consequently larger droplets than the 3-line model (Case 2b). Grouping together bouncing and stretching separation (i.e. grazing) is not problematic here, since no satellite formation is considered. However, if satellite formation is important, a separation between bouncing and stretching separation must be considered. The larger droplets produced by the single-line model due to coalescence also results in a higher number of stretching separation collisions, larger than the sum of the bouncing plus stretching separation number resulting from the 3-line boundary model (see Table 3 and Figure 13). Consequently, a one-line boundary model will remarkably overpredict the produced droplet size.

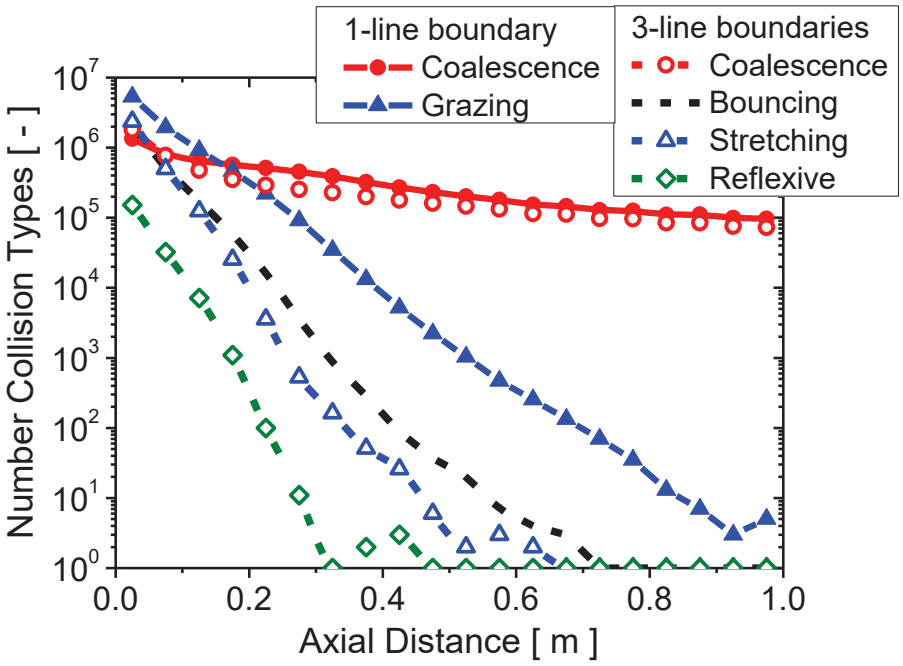

Figure 13: Collision numbers along the spray for the different collision outcomes, with IE and $\Delta = 1$, comparing the SS-C boundary by the B-S model using a 1-line and a 3-line (Figure 8a) model (i.e. Case 2b and 2c).

In any spraying systems the droplets of course have a rather wide size spectrum so that colliding droplets have mostly different sizes and hence the size ratio in the boundary line equations has to be considered. As discussed above, the B-S boundary line reflects the expected behaviour with reduced size ratio much better, especially for $0.5 < \Delta < 1.0$ (Sommerfeld and Pasternak 2019). Therefore, the conditional droplet collision numbers along the spray are compared for the Case 2b with $\Delta = 1$ and the Case 4 with variable Δ (see Figure 8 c) in Figure 14. To recapitulate, with decreasing size ratio the bouncing boundary is shifted upwards and the SS-C as well as the RS-C boundaries move to the right (Cases 2b and 4). Since the region of coalescence increases with decreasing Δ also the number of coalesced droplets increases along the entire spray (Figure 14). Moreover, the region of bouncing is shrinking whereby the bouncing rate is reduced in the initial region of the spray but for $z > 0.4\ m$ becomes larger than for the case with $\Delta = 1$. This might be associated with the fact that the number of small droplets in the initial spray has been reduced as they were captured by larger ones and coalesce. This will reduce the effect of impact efficiency and yield more collisions with large B and hence bouncing occurs. The region of stretching separation (Figure 8 c) is shifted to the right wherewith their number is reduced in the initial spray region when considering boundary lines with variable Δ. The same happens with reflexive separation. In the farther downstream region, the separation number for variable Δ is

increased compared to $\Delta = 1$ due to the initially modified droplet size spectrum. In conclusion, the consideration of the size ratio in the boundary lines is of immense importance and needs to be included for correctly predicting the produced droplet size spectrum. The remarkable increase of coalescence yields much larger droplets produced by the spray. The consideration of size ratio in the A&P correlation for the SS-C boundary will yield much different behaviour and much less coalescence due to the turning of the SS-C boundary with decreasing Δ. An experimental validation for such behaviour for water as droplet liquid (i.e. for very small droplet size ratios) is still not available.

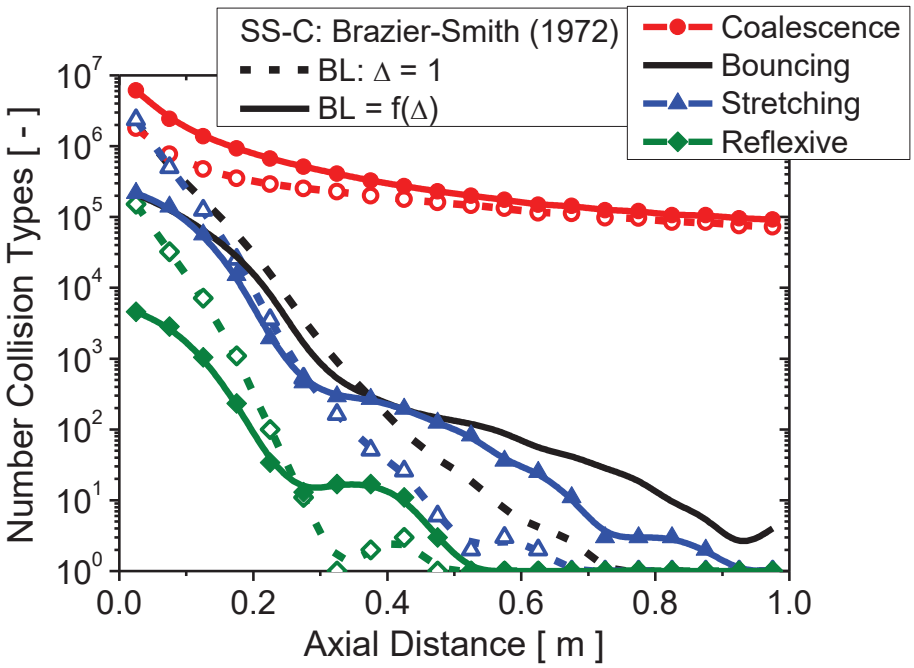

Figure 14: Collision numbers along the spray for the different collision outcomes, with IE and the SS-C boundary by B-S using $\Delta = 1$ and variable Δ (i.e. Case 2b and 4).

Now the situation for liquids with slightly higher dynamic viscosity and reduced surface tension is considered as illustrated in Figure 7 b) for hexanol alcohol as a liquid where bouncing occurs down to $B = 0$ for small *We*. Hence, Case 4 and Case 5 of Table 3 are compared (see also Figure 8d). The collision numbers along the spray for these two cases show drastic changes with regard to the relative importance of bouncing and coalescence (Figure 15). For Case 5 (i.e. bouncing down to $B = 0$) coalescence is drastically diminished whereas bouncing is accordingly augmented. As a result, bouncing is more probable than coalescence in this case. This large influence is caused by the large number of droplet collisions occurring in the domain of small We-numbers (see Figure 11). Reduced coalescence implies a lesser droplet growth whereby also separative collisions are reduced.

This effect will be further discussed below in connection with the Sauter diameter along the spray. Consequently, the structure of the adopted collision map has a drastic influence on the collision outcomes and the produced droplet size spectrum.

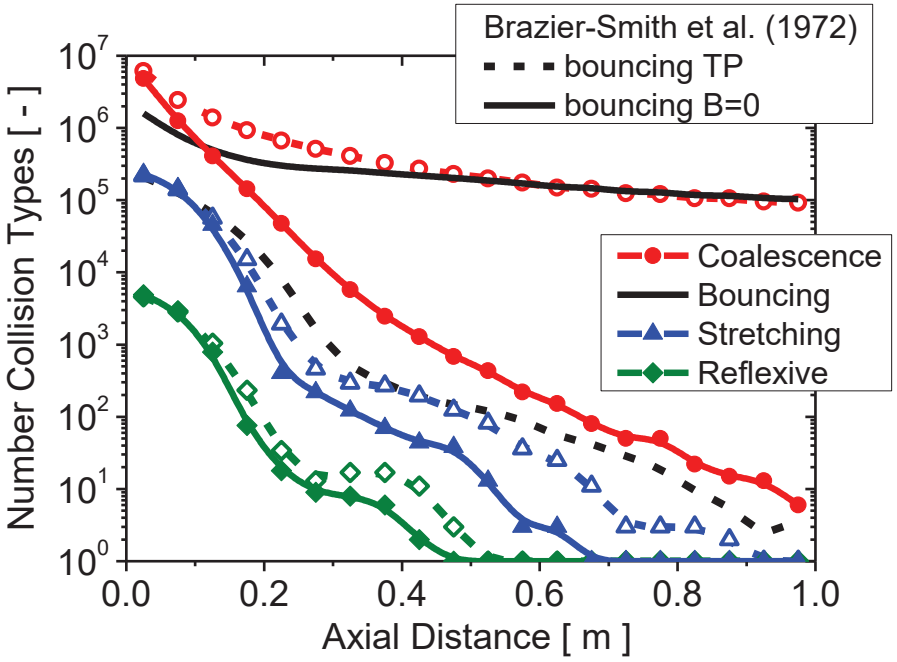

Figure 15: Collision numbers along the spray for the different collision outcomes, with IE and the SS-C boundary by B-S using variable Δ, comparing the bouncing line commencing at the triple point TP (Case 4) and going down to the horizontal axis B=0 (Case 5), see Figure 8 d).

In order to give also an idea about the locations where the different types of droplet collisions occur in a hollow cone spray, Figure 16 provides a graph showing the differences between Case 4 and Case 5, both with the B-S boundary line for SS-C. For a water-type spray (bouncing until the triple point location), coalescence is dominant, occurring along the entire spray (Figure 16a)). Bouncing only is observed in the initial part of the spray, up to about 300 mm. The emerging of stretching covers a similar region and reflexive separation (close to head-on collisions) is only found very near to the nozzle where large relative velocities are observed. Now considering a slightly higher viscosity liquid (i.e. bouncing going down to $B = 0$, see Figure 8d)) bouncing becomes the prevailing collision outcome found along the entire spray (Figure 16b)). This becomes also obvious from the collision density plot in Figure 11b) showing that for low *We* over the entire B-regime the collision number is very high. Coalescence to occur requires now larger Weber numbers and therefore is only found in the initial spray region (i.e. up to about 400 mm), a region with a wider droplet size distribution and a larger relative velocity. Interestingly, a small strip of coalescence is also found near the

centre line up to about 800 mm, which might be caused by small droplet entrainment from the outer regions of the spray. The regions for stretching and reflexive separation in Case 5 are also a bit smaller than for the water-type case (Case 4). From these results it is clear, whenever the boundary lines go through regions of high collision density (see Figure 11), the resulting collision outcomes are very sensitive with regard to the structure of the collision maps.

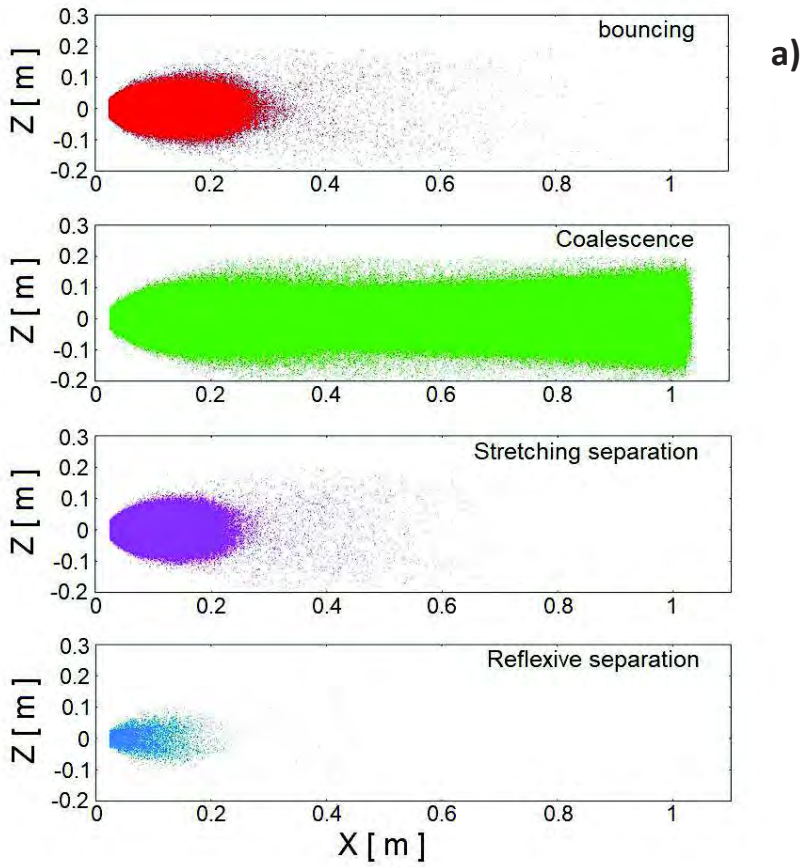

a)

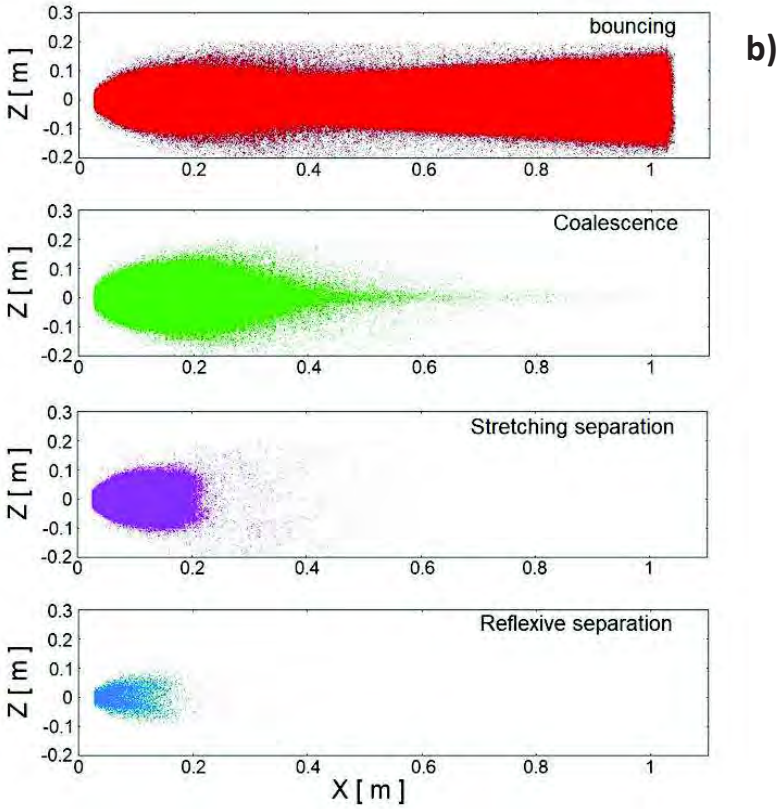

Figure 16: Comparison of the computed droplet collision locations within the spray conditional according to the outcome type comparing **a)** the water-type case (Case 4) and **b)** the case with slightly elevated dynamic viscosity (Case 5), see also Figure 8 d).

A further shift of all boundary lines to the right as a consequence of viscosity increase (Sommerfeld and Kuschel 2016) results in a movement of the region of coalescence to larger Weber numbers. Hence, looking at the collision density plots in Figure 11 the coalescence number is further reduced (compare Case 4 and Case 6 in Figure 17). Bouncing on the other hand further increases but mainly in the initial region of the spray. Due to the shift of all boundary lines to the right also separative collisions are diminished. The observed strong changes of collision numbers through small shifts in the boundary lines of collision maps for spray liquids with different properties reveals the huge sensitivity of this issue on numerical predictions of sprays.

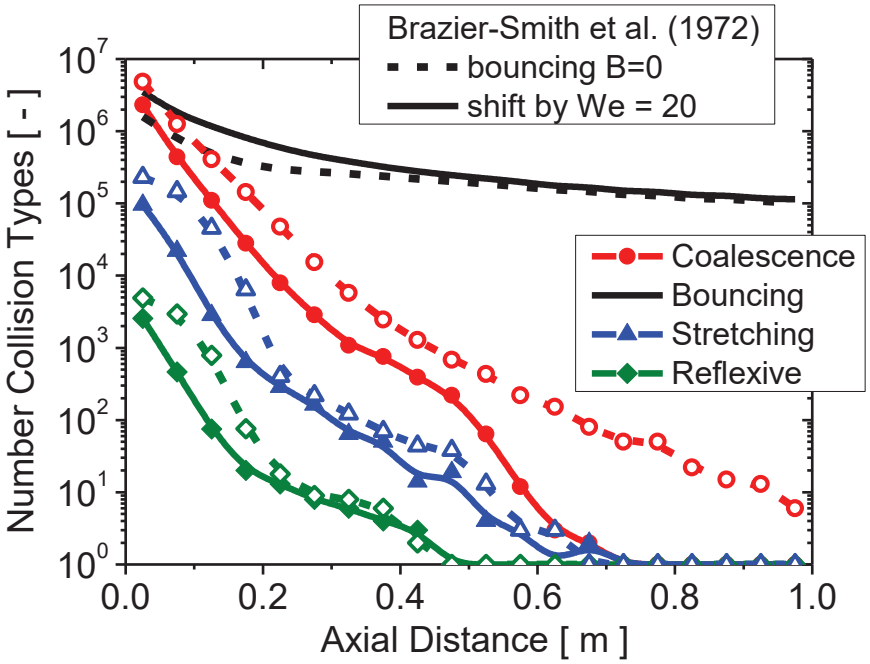

Figure 17: Collision numbers along the spray for the different collision outcomes, with IE and the SS-C boundary by B-S using variable Δ (Case 4) compared with the result where all boundary lines are shifted by, We = 20 (Case 6).

Development of spray droplet sizes

The cross-sectional averaged Sauter mean diameter along the spray is a meaningful way for characterising the performance of the different droplet collision outcome models and to emphasise their importance for a correct prediction of spray development. Essential for most spray applications is of course the produced droplet size spectrum for which a cross-sectional averaging is a compact way of presentation. First a direct comparison of the present simulations with the experimental data and the axisymmetric computations of Rüger et al. (2000) is conducted using the standard droplet collision outcome models (three lines) for the SS-C boundary by A&P (Case 3) as well as B-S (Case 4). For that purpose, only the initial part of the spray up to 600 mm is considered (Figure 18). In the numerical computation without droplet collisions of course the Sauter mean diameter $D_{32,cross}$ should remain constant at about 57 µm, as there is no mechanism for changing droplet size. From 300 mm downstream the nozzle exit however, the $D_{32,cross}$ is being slightly reduced, which is caused by the droplet deposition boundary condition at the walls. Since most likely larger inertial droplet hit the walls, they are removed from the computations. Such a deposition naturally also happens for the other simulations. The development of the $D_{32,cross}$ for the Case 3 and Case 4 (A&P and B-S boundary for SS-C) are very similar but expectedly the B-S model gives

higher values since more coalescence is occurring due to the different SS-C boundary lines (see also Figure 8 a)). The experimental results however show still larger Sauter diameters, a similar trend as observed by Rüger et al. (2000), which may be associated with problems in accurately measuring dispersed phase concentrations or mass flux by a PDA-system (see e.g. Sommerfeld and Tropea 2000). On the other hand, the simulation results of Rüger et al. (2000) with the B-S single boundary line (as Case 2c in Table 3) shows the same curve progression as the present results, but are slightly below the present simulations (three-line boundaries, Case 4) with almost the same slope. Moreover, in the collision model of Rüger et al. (2000) no impact efficiency was considered.

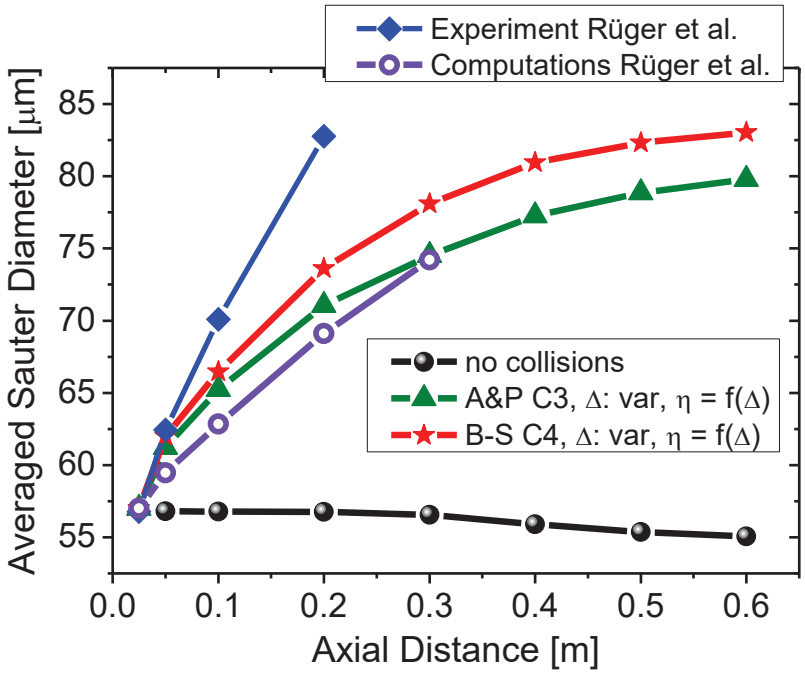

Figure 18: Cross-sectional averaged Sauter mean diameter along the spray, comparison of simulations with no collisions with those for Case 3 (SS-C boundary by A&P) and Case 4 (SS-C boundary by B-S) as well as those presented by Rüger et al. (2000), experiments and Euler/Lagrange computations.

In order to illustrate the influence of the different droplet collision map structures based on the B-S boundary line for SS-C, Figure 19 gives a detailed summary. As previously shown, impact efficiency (IE) reduces collision rates within the considered spray, however, only slightly coalescence and more pronounced bouncing rates (see Figure 10). Consequently, the Sauter mean diameter is only slightly reduced when accounting for IE (compare C1b and C2b in Figure 19). In addition, IE reduces mainly the probability of small droplets not hitting the collector. Just using a single line boundary model as used by Rüger et al. (2000), gives again larger Sauter mean diameter due to more coalescence (i.e. missing of reflexive separation), but this is still a bit smaller than for the full 3-line boundary model (compare C2c and C4 in

Figure 19). Thereby, the present results for Case 2c come closer to the numerical result of Rüger et al. (2000).

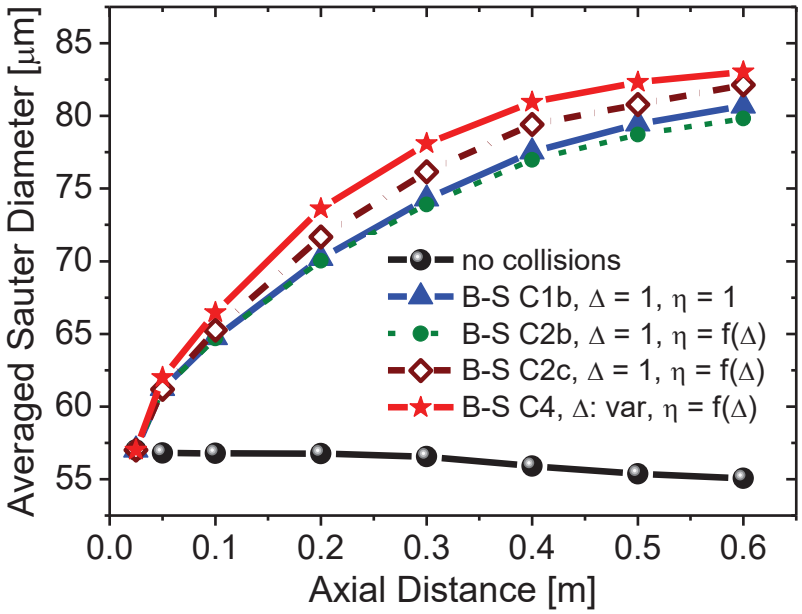

Figure 19: Cross-sectional averaged Sauter mean diameter along the spray, comparison of simulations with no collisions with those for using the SS-C boundary by B-S in connection with different collision maps: Case 1b and Case 2b are 3-line boundary models without and with IE, Case 2c is a single line boundary model and Case 4 the full three-line boundary model with the B-S boundary for SS-C using variable Δ.

The influence of different collision outcome maps on the predicted Sauter mean diameter $D_{32,cross}$ is further considered in Figure 20 for the Case 0, Case 4, Case 5 and Case 6. Regarding these spray simulations it was assumed that the droplets have a specular reflection at the walls in order to obtain a result where the Sauter diameter is not affected by the disappearance of droplets and hence in Case 0 is almost constant. For the standard water-type condition in Case 4, where the bouncing boundary ends at the triple point, and due to the strong coalescence occurring in the spray, a remarkable growth of the Sauter mean diameter is found, but now due to the rebound wall boundary condition the $D_{32,cross}$ reaches more than 85 µm (compare with Figure 18). If the bouncing boundary goes down to $B = 0$ being observed for a slightly more viscous liquid (see Figure 7 and Figure 8d)), coalescence is strongly diminished and most of the collisions result in bouncing (see Figure 15). Consequently, the $D_{32,cross}$ increases rapidly until 50 to 100 mm downstream the nozzle exit and then remains almost constant (Figure 20). For the Case 6 where all boundary lines are shifted by $We = +20$ in order to mimic an even higher viscous liquid (see Figure 8 e) and Figure 7 for hexanol), the

coalescence rate is further reduced and already after 50 mm the Sauter mean diameter remains constant.

In conclusion, essential for predicting the droplet size evolution in a spray is the assumed droplet collision map. Approximations to the realistic collision map may yield remarkable errors. Besides that, additionally the collision density plot (see Figure 11) is very important, which is largely depending on the characteristics of the spray nozzle. Basically, the superimposing of collision map and collision density plot gives an indication about which type of collision is important.

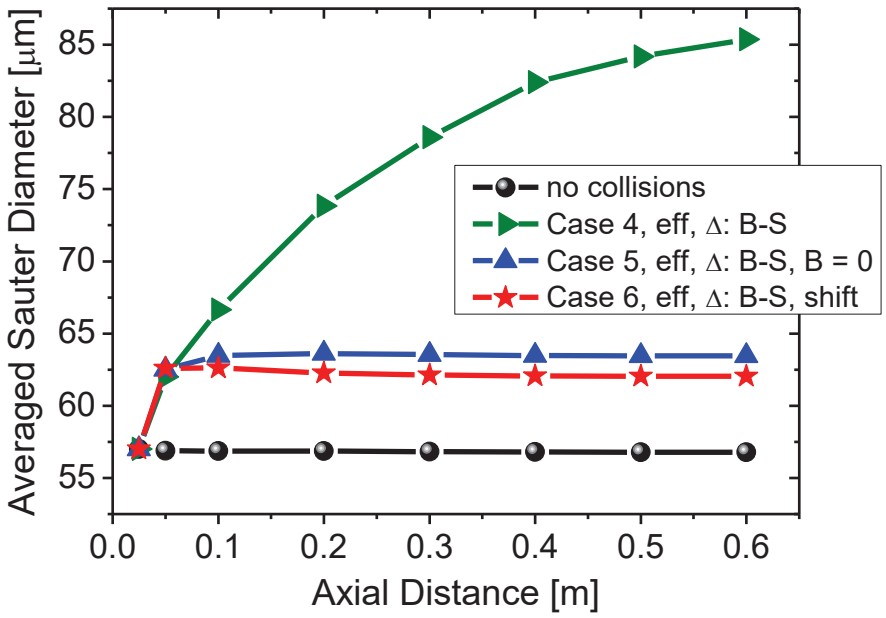

Figure 20: Cross-sectional averaged Sauter mean diameter along the spray, comparison of simulations for no collisions with those for Case 4 (SS-C boundary by B-S) as well as those predicted by the Case 5 and Case 6 using a specular reflection of the droplets at the wall.

The changes in Sauter mean diameter development along the spray are remarkable and strongly depend on the presumed collision map. In which way a local droplet size distribution within the spray is modified by the collision map assumption is shown in Figure 21 for the mass-based droplet size PDF. Using the A&P correlation for the SS-C boundary (Case 3), gives already a notable shift of the PDF to the right compared to the result neglecting droplet collisions. As mentioned before, the B-S boundary is more realistic for water (Case 4) and yields an even higher rate of coalescence causing a broadening and a further displacement of the PDF to larger droplets. Applying the collision map of Case 5 (i.e. bouncing going down to $B = 0$) the mass-based size PDF (Figure 21) is again shifted back to almost the same result as for the case without collisions (Case 0). Even the number of smaller droplets becomes slightly

higher, although the Sauter mean diameter is somewhat larger (see Figure 20). Naturally, the local droplet size distribution is not only affected by coalescence, but also through the size-dependent transport of the droplets by the gas phase.

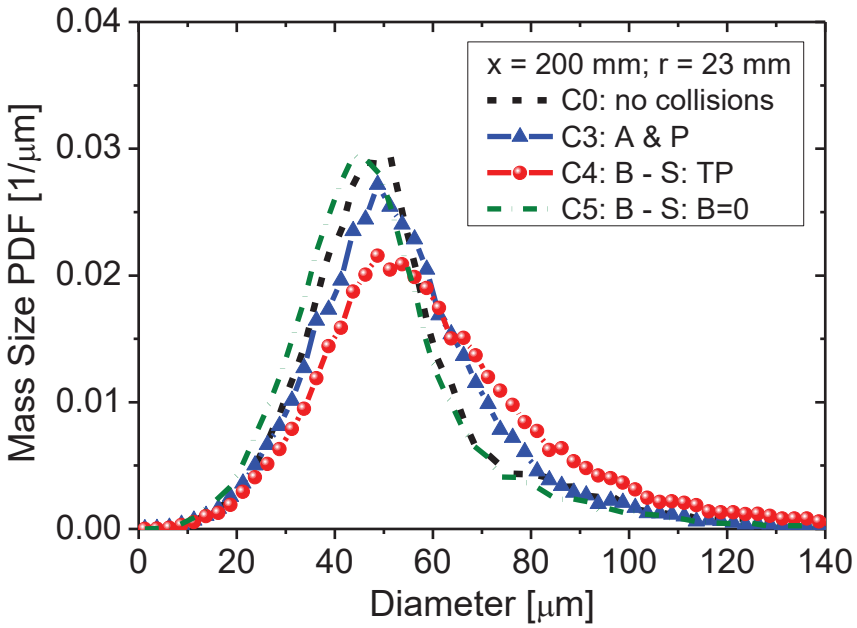

Figure 21: Comparison of the droplet mass-based size distributions obtained through numerical computations with different assumptions and presumed collision maps; no collisions Case 0, with the three-line boundary collision map and the SS-C boundary by A&P (Case 3) as well as B-S (Case 4) and the Case 5 with bouncing going down to b = 0; location: x = 200 mm, r = 23 mm.

Droplet collision size ratio

In the considered spray, the initial droplet size distribution is rather wide and in addition the size PDF changes with the radius of injection (see Figure 24 b); the mean number diameter changes from about 10 to 45 μm). Therefore, collisions between droplets will mostly occur with different sized droplets. In addition, the relative velocity between small and large droplets is of course much higher due to their different response to the gas flow field, or due to their different inertia when ejected from the nozzle with the same velocity. The numerical simulations now allow determining the PDFs of the droplet size ratio Δ (see Eq. 4) just upon collision. Such PDFs were determined by sampling and averaging the values for the various cross-sections along the spray. The largest droplet collision rates are in the initial region of the spray (compare Figure 16) where most likely large and fast droplets capture small and slower ones so that the collision size ratio is initially quite small. In Figure 22a) these size ratio PDFs are shown for the Case 1b (i.e. the SS-C boundary is expressed by B-S and the impact efficiency (IE) is not considered) indicating that initially (x = 50 mm) the PDF has a

maximum at around $\Delta = 0.1$. Going further downstream the spray, of course the droplets grow due to coalescence and small droplets disappear. As a consequence, the collision size ratio is shifted to larger values and eventually spans the entire range between 0 and 1. However, the probability of equal sized droplet collisions is only 0.5% (Figure 22a). If now the IE is accounted for in the collision model, a number of smaller droplets will not collide with the larger (collector) droplet since they will move around the collector with the relative flow. As a result, the probability of small size ratios upon collision is reduced for all planes along the spray (Figure 22b).

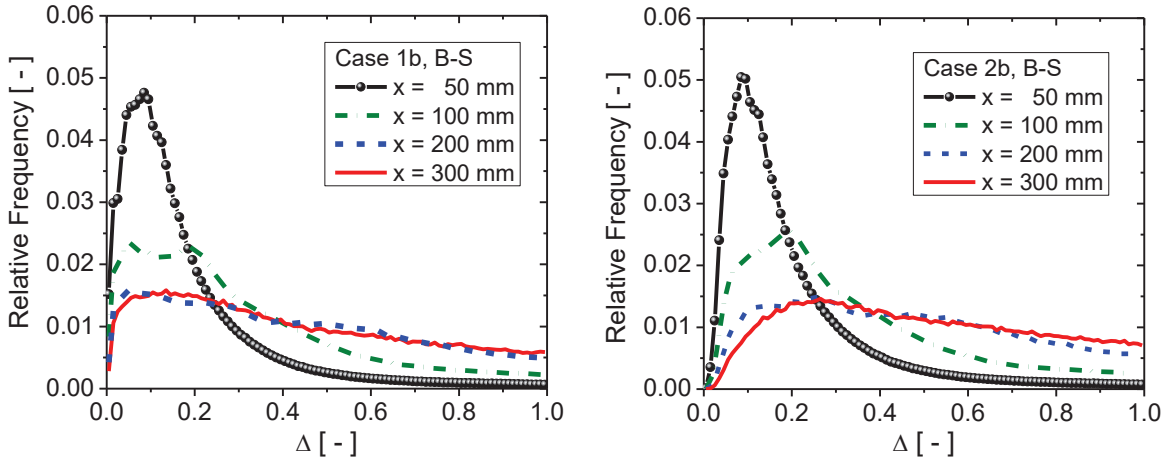

Figure 22: Cross-section-wise sampled collision size ratio PDFs along the spray (i.e. from x = 50 mm to x = 300 mm) obtained from the simulations using the three-line collision map with the SS-C boundary by B-S for **a) Case 1b** with $\Delta = 1$ but without IE and **b) Case 2b** with $\Delta = 1$ and also considering IE.

Now the more realistic case with the three-line collision maps and all boundary lines depending on the droplet size ratio upon collision and accounting for impact efficiency is considered, namely water-type, Case 4. According to the type of collision outcome for this case, the size ratio PDFs are conditionally extracted for all collision types, as well as for bouncing, coalescence and stretching (Figure 23). The total size ratio PDFs are of course very similar to those for coalescence, since for Case 4 this type of collision is dominant (see also Figure 14). Most of the collisions occur at small size ratio with a shift of the PDFs to larger Δ when moving along the spray due to the number of small droplets being reduced through coalescence. Consequently, the highest probabilities exist for collision droplet size ratios between 0 and 0.4. Both bouncing and stretching separation occur at slightly higher Weber numbers (i.e. $We > 10$ for $\Delta = 1$, see Figure 8a) and d)) being associated with larger droplets. As a result, the collision size ratio PDFs begin at higher Δ (i.e. $\Delta > 0.2$) having a similar maximum for bouncing and stretching in the range $0.33 < \Delta < 0.5$, depending on the cross-

section within the spray. Since it is more likely that small droplets are captured by collisions, the maximum is shifted to larger Δ when going down the spray. At the last cross-section both PDFs show strong oscillations due to the much smaller number of bouncing and stretching collision events (see Figure 16 a).

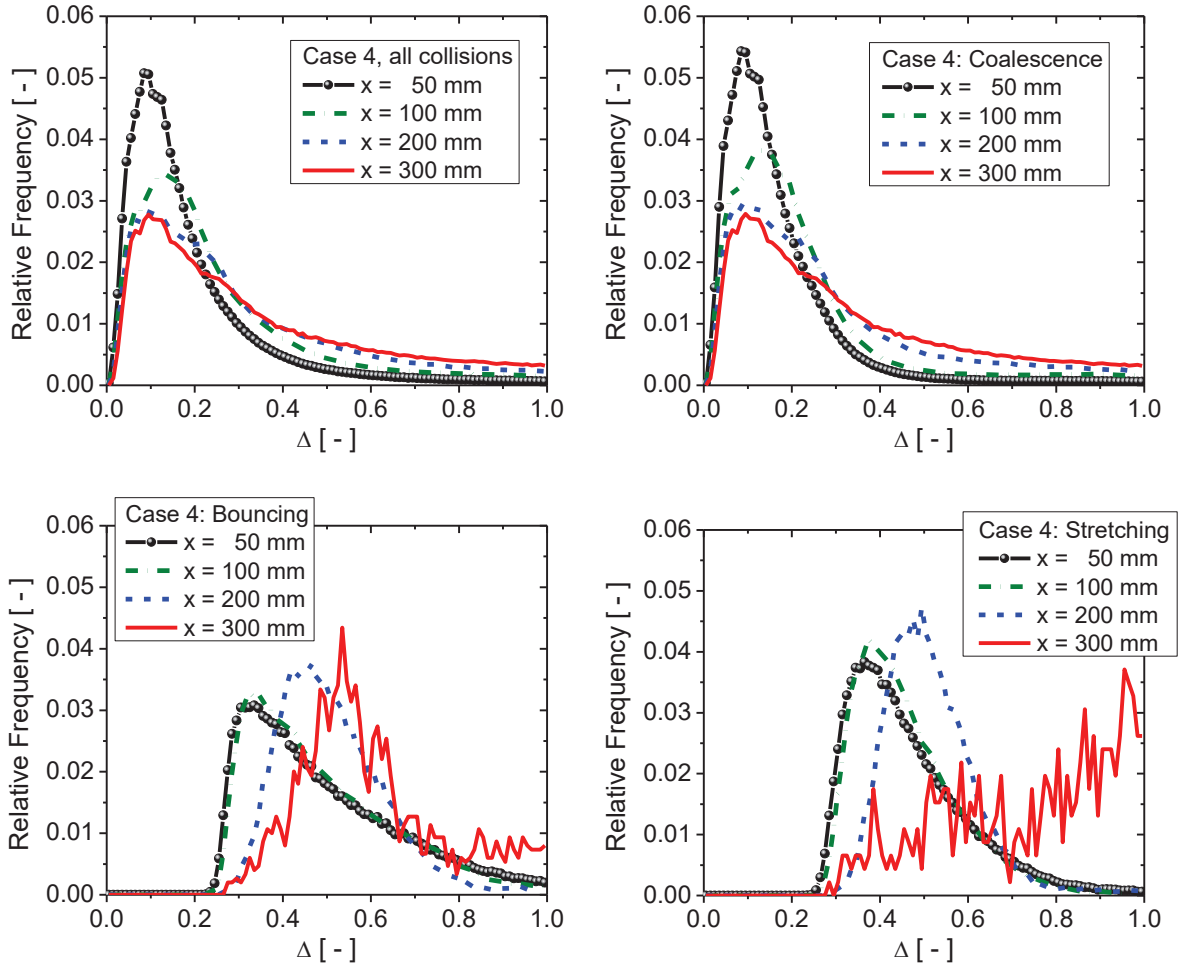

Figure 23: Cross-section-wise sampled collision size ratio PDFs along the spray (i.e. from x = 50 mm to x = 300 mm) obtained from the simulations of Case 4 using the three-line collision map with the SS-C boundary by B-S; **a) all collisions, b) coalescence, c) bouncing, d) stretching separation**.

These results clearly confirm that small size ratio collisions are dominant. For this regime (i.e. $\Delta < 0.3$) almost no experimental studies are available for validating theoretical correlations for the boundary lines. The experiments of Sommerfeld and Pasternak (2019) for polymer solutions and sun flower oil were conducted down to a size ratio of about $\Delta \approx 0.34$. The proposed composite boundary line for SS-C works reasonably well for size ratios $0.5 < \Delta < 1.0$, however failed to capture the experimental boundary for $\Delta \approx 0.34$. This also indicates the need for further theoretical studies on small size ratio droplet collisions.

Comparison of the spray computations with experiments

The experimental data of Rüger et al. (2000) not only allowed to specify exact gas phase and spray inlet conditions, but also provided a number of profiles for gas and droplet phase properties (i.e. at 25, 50, 100 and 200 mm downstream of the geometrical nozzle exit). In Figure 24 the droplet properties obtained without droplet collisions (Case 0) and with collisions and coalescence using the tree-line boundary model with the B-S line for SS-C boundary (Case 4 in Table 3) are compared with the measurements. Both simulations were conducted with full two-way coupling as described above. Generally, the agreement with the experiments is excellent for the spray until 100 mm downstream of the nozzle exit. Only for the profiles x = 200 mm some larger differences between the simulations and measurements are observed. The predicted radial spread of the spray (Figure 24d) seems to be slightly underpredicted which has of course a consequence for the concentration profile (Figure 24a) and the droplet number mean diameter (Figure 24b). The overprediction of the droplet size was also found by Rüger et al. (2000). Although the predicted Sauter mean diameter for Case 0 (no collisions) compared to Case 4 (with collisions and coalescence) shows at the streamwise $x = 200\ mm$ an increase of about 15 µm (see Figure 20 axial distance 0.2m), such a difference is not visible in the profiles of the number-based mean diameter (Figure 24b). Naturally, the number-based droplet diameter (Figure 24b) is less sensitive against the effect of droplet coalescence. For a single coalescence the number in a larger droplet size class is only increased by one, whereas for a mass-based size distribution the mass or volume in that class is increased by the diameter cubed (compare Figure 25 with Figure 21). In Figure 25, two measured number-based droplet size distributions from the core region of the spray are compared with numerical computations without (Case 0) and with coalescence (Case 4). Nevertheless, even in this dilute spray, the effect of coalescence is clearly visible and the number of larger droplets is slightly increasing and accordingly smaller droplets are reduced in number. The agreement with the measurements for these two locations is also quite good.

Most of the profiles presented in Figure 24 show virtually only small difference between the Case 0 (without collisions) and Case 4 (with collision using the B-S boundary for SS-C), also for the axial and radial droplet velocities. Again, it should be remarked, that the profiles are all based on ensemble averaging, namely based on droplet number counts. In addition, the considered spray is rather dilute, so that not very many collisions occur to yield remarkable differences in the droplet velocities. However, inspecting in more detail, reveals that for the profiles at 100 and 200 mm downstream of the nozzle exit and towards the outer edge of the spray, mean velocity components are slightly reduced and also droplet fluctuating energy (i.e.

defined as $k_P = 0.5\,(u_{Prms}^2 + 2\,v_{Prms}^2)$) more distinct (Figure 24e). Since the droplets become larger due to coalescence (Case 4) they of course will respond at a lesser extent to the mean gas flow and turbulence.

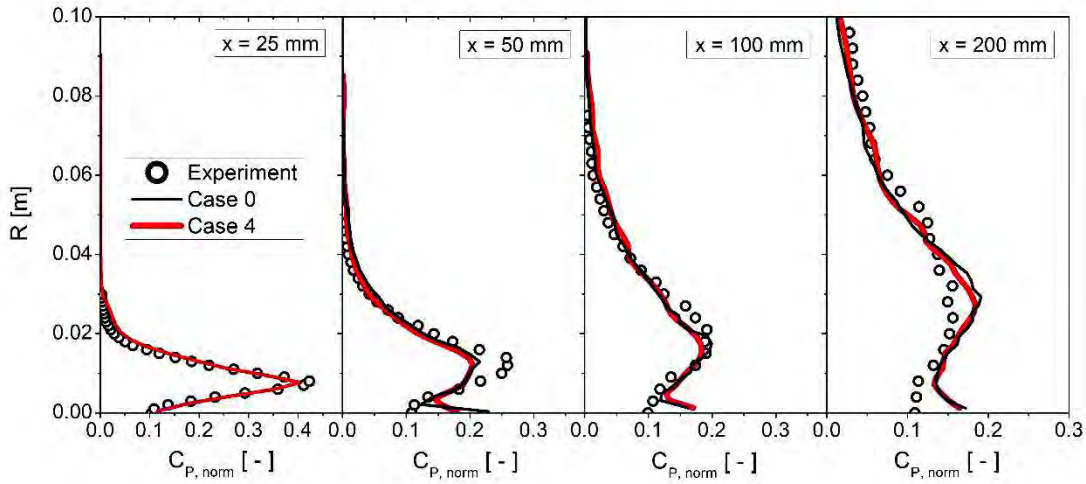

a)

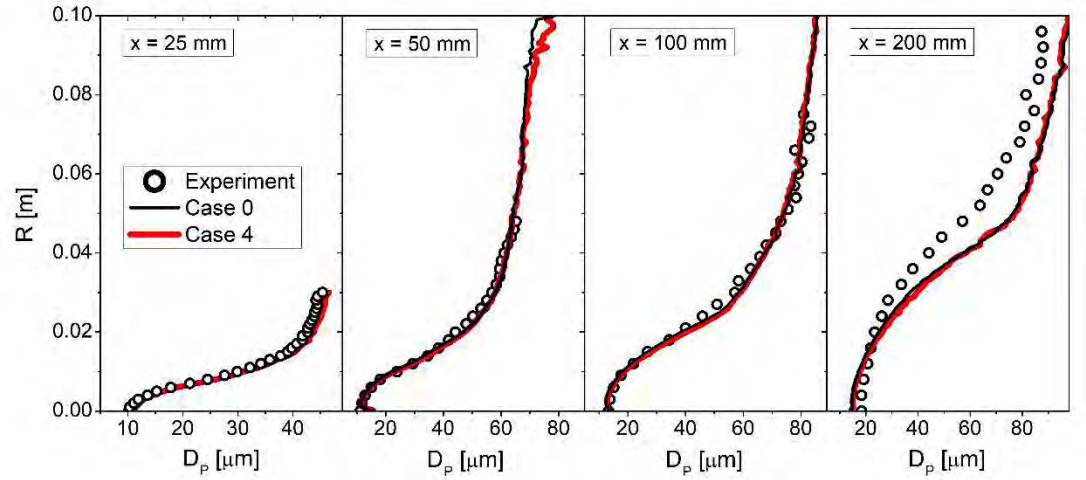

b)

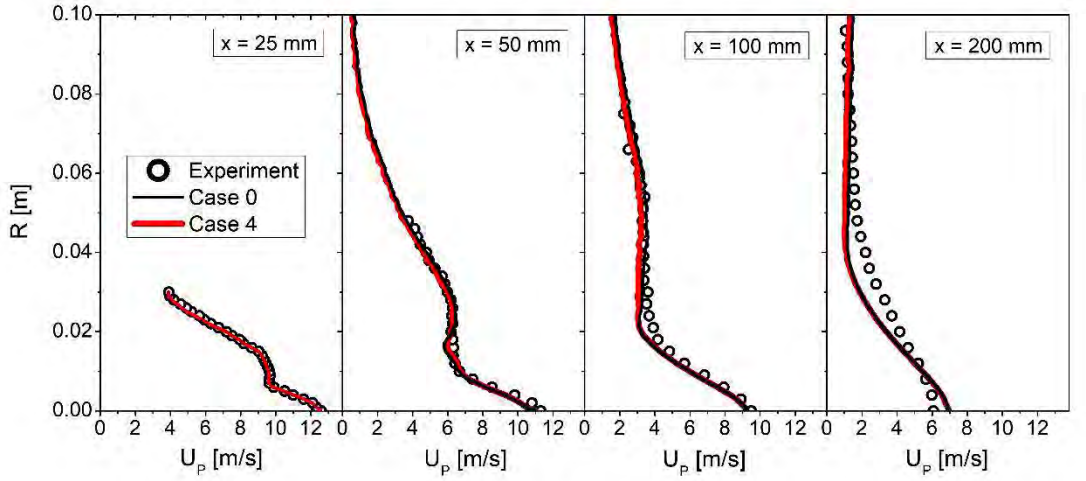

c)

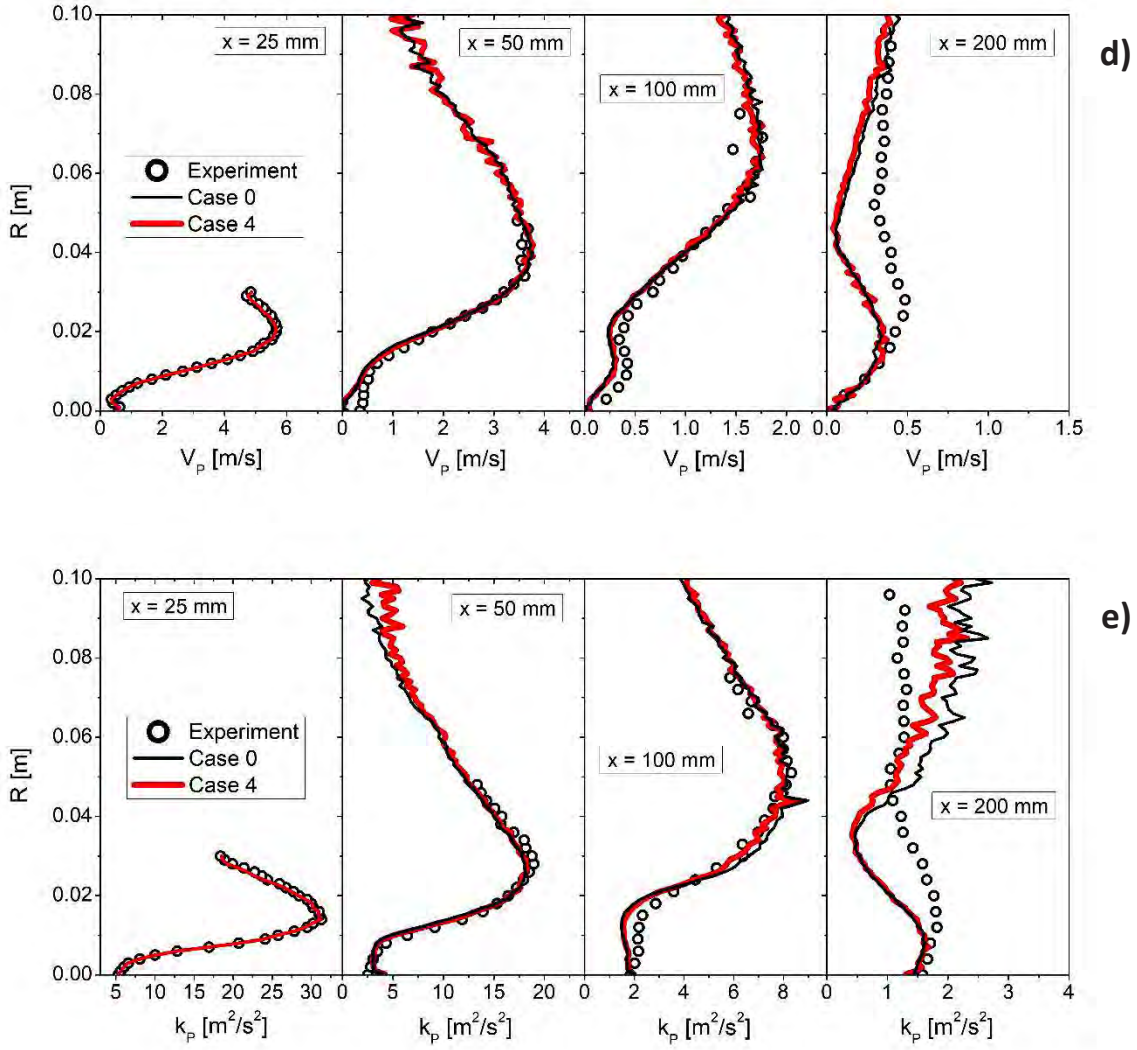

Figure 24: Comparison of measured profiles of the droplet phase properties with simulation results for the case without droplet collisions (Case 0) and for the Case 4 with the three-line boundary collision map (SS-C boundary by B-S), according to Table 3; a) droplet concentration, b) droplet number mean diameter, c) droplet axial mean velocity, d) droplet radial mean velocity and e) fluctuating energy of droplets.

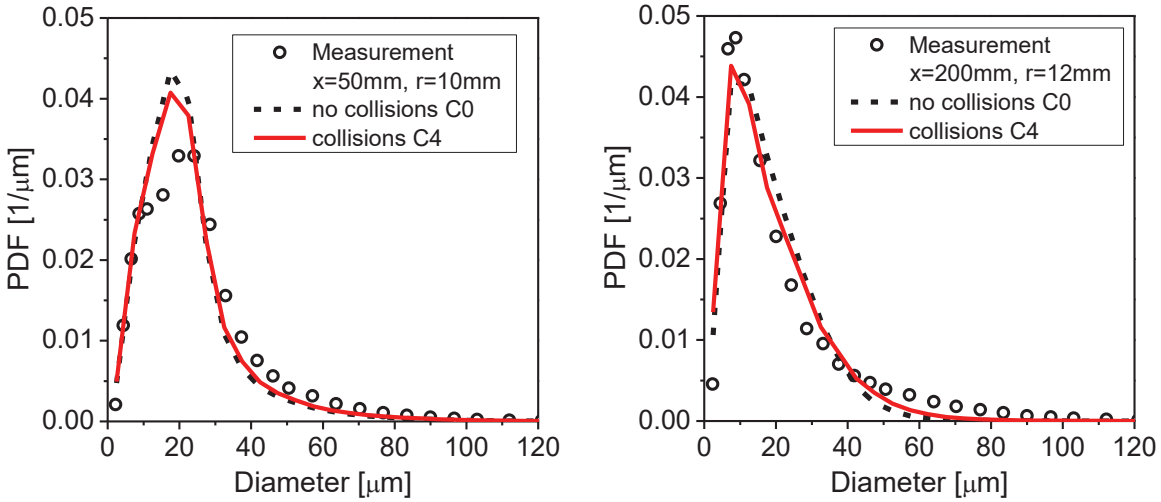

Figure 25: Comparison of measured local droplet number-based size distributions with numerical results for the cases without (Case 0) and with coalescence (Case 4 with the three-line boundary collision map, SS-C boundary by B-S); location left: x = 50 mm, r = 10 mm; right: x = 200 mm, r = 12 mm.

4 Conclusions

Even in reasonably dilute sprays, droplet collisions and the resulting possible coalescence have a remarkable influence on the developing droplet size spectrum, however not so much on the droplet velocities. Therefore, in a numerical computation of spraying systems, which is preferably done by an Euler/Lagrange approach, droplet collisions need to be modelled properly including all relevant sub-steps, namely collision detection, impact efficiency and collision outcome specification. For deciding on the outcome of binary droplet collisions, so-called collision maps are being used which distinguish in the lower Weber-number regime between bouncing, coalescence and stretching as well as reflexive separation, and are mainly based on experimental supported theoretical derived boundary lines. The structure of a collision map strongly depends on droplet size ratio and the liquid properties, implying that different collision maps have to be used for different applications; e.g. spray cooling, spray combustion or spray drying. In the present article, the influence of the presumed collision maps on the collision rates for the different outcomes and the eventually produced droplet size spectrum was analysed in detail using numerical predictions through the Euler/Lagrange approach applied to a stationary hollow-cone spray. The droplet collision model was based on the fully stochastic approach, supplemented by the important impact efficiency, correlated velocities of the fictitious collision partner and a collision outcome map. It was first of all demonstrated that such an efficient fully stochastic collision model is very accurate and the obtained collision frequencies are largely independent of mesh size, tracked number of parcels

and also the applied Lagrangian tracking time step size. The comparison of the numerical results for a number of different presumed model settings and collision maps with respect to the total and the conditional collision numbers, as well as the produced droplet sizes allow for the following conclusions and suggestions:

- The consideration of impact efficiency gives overall much lower collision numbers and reduces the number of collisions with larger B and thereby bouncing as well as coalescing collisions; the resulting Sauter mean diameter is however only slightly lower than without IE, since impact efficiency mainly reduces collisions of small droplets.
- The standard three-line collision map with the B-S (Brazier-Smith et al. 1972) correlation for the SS-C (stretching separation-coalescence) dividing line yields much less bouncing and increases coalescence compared to the A&P (Ashgriz and Poo 1990) boundary.
- The B-S boundary line for SS-C is more realistic than the A&P one for water and shows a better and more realistic behaviour for decreasing size ratio Δ (see Sommerfeld and Pasternak 2019).
- For a water type collision map using B-S for the SS-C boundary yields a 30 µm bigger Sauter mean diameter compared to a simulation without collisions.
- Applying only a single-line collision map (i.e. just for SS-C boundary) gives more coalescence due to neglecting reflexive separation and therefore a larger Sauter mean diameter will result.
- The consideration of variable size ratio (i.e. Δ) in the boundary lines reduces bouncing and enhances coalescence giving again an increase in Sauter mean diameter at the end of the spray.
- If bouncing is going down to $B = 0$ at small We number (i.e. observed for many slightly higher viscous liquids like alkanes, alcohols and light oils) one obtains much more bouncing and accordingly much less coalescence so that the Sauter mean diameter becomes only about 6 µm, larger than without considering droplet collisions, but more than 20 µm smaller than for a water-type collision map (i.e. bouncing only going to the triple point).
- The superposition of a collision density plot (i.e. occurrence of collisions in a $B = f(We)$ plane which is quite specific for the type of spray nozzle considered) with the collision map gives a good indication of which type of collision outcomes are relevant.
- Whenever, a boundary line goes through a region of high collision density, the collision outcomes are very sensitive with regard to small changes of the boundary lines, for example through changes of size ratio.

- It was found that for the considered hollow-cone spray (i.e. droplet size distribution) the majority of collisions occur with size ratios between $0.1 < \Delta < 0.3$. For this regime an experimental verification of the boundary lines is completely missing for any type of liquid.
- The collision map with the B-S correlation for the SS-C boundary was found previously (Sommerfeld and Pasternak 2019) to provide meaningful results for droplet size ratios between $0.5 > \Delta > 1.0$.
- The computed results using the three-line collision map with B-S correlation for the SS-C boundary showed excellent agreements with the measurements regarding droplet concentration and droplet velocities as well as local droplet size distributions.
- The predicted velocity profiles of both phases are less sensitive with regard to the selected collision map, since number-based properties in a dilute spray are not very distinctively influenced.
- The numerically predicted local mass-based droplet size distributions are on the other hand strongly influenced by coalescence and hence the selected collision map.
- Any crude approximations of the collision map for the real liquid type in the spray will not provide correct results.

Acknowledgements

The authors acknowledge the financial support for part of this research project through the Deutsche Forschungsgemeinschaft (DFG) under contract SO 204/35-1 to 3.

References

Amsden, A.A., O`Rourke, P.J. and Butler, T.D.: KIVA-II: A computer program for chemically reactive flows with sprays. Los Alamos Scientific Laboratory Report, LA-11560-MS (1989)

Ashgriz, N. and Poo, J.Y.: Coalescence and separation in binary collisions of liquid drops. Journal of Fluid Mechanics, Vol. 221, 183 – 204 (1990)

Bauman, S.D.: A spray model for an adaptive mesh refinement code. Ph.D. Thesis University of Wisconsin-Madison (2001)

Brazier-Smith, P. R., Jennings, S. G. and Latham, J.: The interaction of falling water drops: coalescence. Proc. R. Soc. Lond. A, Vol. 326, 393 – 408 (1972)

Crowe, C.T., Sharma, M.P. and Stock, D.E.: The Particle-source-in-cell (PSI-cell) model for gas-droplet flows. J. of Fluids Eng. Vol. 99, 325-332 (1977).

Dukowicz, J.K.: A particle-fluid numerical model for liquid sprays. J. of Computational Physics, Vol. 35, 229 – 253 (1980)

Estrade, J.-P., Carentz, H., Lavergne, G., Biscos, Y.: Experimental investigation of dynamic binary collision of ethanol droplets - a model for droplet coalescence and bouncing. International Journal of Heat and Fluid Flow, Vol. 20, 486 – 491 (1999)

Finotello, G., Padding, J.T., Buist, K.A., Jongsma, A., Innings, F. and Kuipers, J.A.M.: Droplet collisions of water and milk in a spray with Langevin turbulence dispersion. International Journal of Multiphase Flow, Vol. 114, 154 – 167 (2019)

Foissac, A., Malet, J., Mimouni, S. and Feuillebois, F.: Binary water droplet collision study in presence of solid aerosols in air. Proceedings 7th International Conference on Multiphase Flow, ICMF2010, Tampa, FL USA, may 30. – June 4. 2010

Fritsching, U.: Spray Simulation: Modeling and Numerical Simulation of Spray Forming Metals. Cambridge University Press (2004)

Gavaises, T.L. Theodorakakos, A. Bergerles, G. and Brenn, G.: Evaluation of the effect of droplet collisions on spray mixing. Proc. Inst. Mechanical Engineers, Vol. 210, 465 – 465 (1996)

Göz, M.F., Lain, S. and Sommerfeld, M.: Study of the Numerical Instabilities in Lagrangian Tracking of Bubbles and Particles in Two-Phase Flow. Computers and Chemical Engineering, Vol. 28, 2727 – 2733 (2004)

Guo, B. Fletcher, D.F. and Langrish, T.A.G.: Simulation of the agglomeration in a spray using Lagrangian particle tracking. Applied Mathematical Modelling, Vol. 28, 273 – 290 (2004)

Ho, C.A. and Sommerfeld, M.: Modelling of micro-particle agglomeration in turbulent flow. Chem. Eng. Sci., Vol. 57, 3073 – 3084 (2002)

Jiang, Y. J., Umemura, A. and Law, C.K.: An experimental investigation on the collision behavior of hydrocarbon droplets. Journal of Fluid Mechanics, Vol. 234, 171 – 190 (1992)

Kim, S., Lee, D.J. and Lee, C.S.: Modeling of binary collisions for application to inter-impingement sprays. Int. J. Multiphase Flow, Vol. 35, 533 – 549 (2009)

Ko, G.H. und Ryou H.S.: Modeling of droplet collision-induced breakup process. Int. J. Multiphase Flow, Vol. 31, 723 – 738 (2005)

Kolakaluri, R., Subramaniam, S. and Panchagnula, M.V.: Trends in multiphase modelling and spray simulations. Int. J. of Spray and Combustion Dynamics, Vol. 6, 317 – 356 (2014)

Kollar, L. Farzaneh, M. and Karev, A.R.: Modeling droplet collisions and coalescence in an icing wind tunnel and the influence of these processes on droplet size distribution. Int. J. Multiphase Flow, Vol. 31, 69 – 92 (2005).

Kohnen, G., Rüger, M. and Sommerfeld, M. Convergence behaviour for numerical calculations by the Euler/Lagrange method for strongly coupled phases. Num. Meth. for Multiphase Flows, FED vol. 185. Eds: Crowe et al., 191-202 (1994).

Kohnen, G. and Sommerfeld, M. The effect of turbulence modelling on turbulence modification in two-phase flows using the Euler–Lagrange approach, Proc. 11th Symp. on Turbulent Shear Flows, Grenoble (France), vol. 2, P3, 23–28 (1997).

Kuschel, M. and Sommerfeld, M.: Investigation of droplet collisions for solutions with different solids content. Experiments in Fluids, Vol. 54, 1440 (2013)

Laín, S., Sommerfeld, M. and Kussin, J. Experimental studies and modelling of four-way coupling in particle-laden horizontal channel flow. Int. J. Heat and Fluid Flow, vol. 23, 647-656 (2002).

Lain, S.: On modelling and numerical computation of industrial dispersed two-phase flow with the Euler-Lagrange approach. Habilitation Martin-Luther-University Halle-Wittenberg, Shaker Verlag, Aachen (2010)

Lain, S. and Sommerfeld, M.: Characterisation of pneumatic conveying systems using the Euler/Lagrange approach. Powder Technology, Vol. 235, 764 – 782 (2013)

Merci, B. and Gutheil, E. (Eds.): Experiments and Numerical Simulations of Turbulent Combustion of Diluted Sprays. ERCOFTAC Series, Vol. 19, Springer International Publishing Switzerland (2014)

Munnannur, A. and Reitz, R. D.: A new predictive model for fragmenting and non-fragmenting binary droplet collisions. Int. J. Multiphase Flow, Vol. 33, 873 – 896 (2007)

Nijdam, J.J., Guo, B., Fletcher, D.F. and Langrish, T.A.G.: Lagrangian and Eulerian models for simulating turbulent dispersion and coalescence of droplets within a spray. Applied Mathematical Modelling, Vol. 30, 1196 – 1211 (2006)

Nordin N.: Complex chemistry modeling of diesel spray combustion. Ph.D. Thesis, Chalmers University of Technology (2001)

O´Rourke P.J.: Collective drop effects on vaporizing liquid sprays. *Dissertation*, Los Alamos National Laboratory, New Mexico (1981)

O`Rourke, P.J. and Amsden, A.A.: The TAB method for numerical calculation of spray droplet breakup. SAE Paper 872089 (1987)

Perini, F. and Reitz, R.D.: Improved atomization, collision and sub-grid scale momentum coupling models for transient vaporizing engine sprays. Int. J. Multiphase Flow, Vol. 79, 107 – 123 (2016)

Pischke, P., Kneer, R. and Schmidt, D.P.: A comparative validation of concepts for collision algorithms for stochastic particle tracking. Computers & Fluids, Vol. 113, 77 – 86 (2015)

Platzer, E. and Sommerfeld, M.: Modeling of turbulent atomization combining a two-fluid and a structure function approach. Atomization and Sprays, Vol. 16, 103 – 126 (2006)

Post, S. L. and Abraham, J.: Modeling the outcome of drop-drop collisions in Diesel sprays. International Journal of Multiphase Flow, Vol. 28, 997 – 1019 (2002)

Qian, J. and Law, C.K.: Regimes of coalescence and separation in droplet collision. Journal of Fluid Mechanics, Vol. 331, 59 – 80 (1997)

Rüger, M., Hohmann, S., Sommerfeld, M. and Kohnen, G. Euler/Lagrange calculations of turbulent sprays: The effect of droplet collisions and coalescence. Atomization and Sprays, Vol. 10, 47 – 81 (2000)

Schiller, L. and Naumann, A. Über die grundlegenden Berechnungen bei der Schwerkraftaufbereitung. Z. Ver. Deut. Ing., Vol. 77, 318 – 320 (1933).

Schmidt D.P. and Rutland C.J.: A new droplet collision algorithm. J. Comp. Phys. Vol.164, 62 – 80 (2000)

Schuch, G. und Löffler, F.: Über die Abscheidewahrscheinlichkeit von Feststoffpartikeln an Tropfen in einer Gasströmung durch Trägheitseffekte. Verfahrenstechnik Vol. 12, 302-306 (1978)

Sommerfeld, M. and Zivkovic, G. (invited lecture): Recent advances in the numerical simulation of pneumatic conveying through pipe systems. *Computational Methods in Applied Science* (Eds. Ch. Hirsch, J. Periaux and E. Onate) Invited Lectures and Special Technological Sessions of the First European Computational Fluid Dynamics Conference and the First European Conference on Numerical Methods in Engineering, Brussels, Elsevier Amsterdam, pp. 201-212 (1992)

Sommerfeld, M. and Tropea, C.: Single-Point Laser Measurement. Chapter 7 in Instrumentation for Fluid-Particle Flow (Ed. S.L. Soo), Noyes Publications, 252 – 317 (1999)

Sommerfeld, M.: Validation of a stochastic Lagrangian modelling approach for inter-particle collisions in homogeneous isotropic turbulence". Int. J. of Multiphase Flows, Vol. 27, 1828 – 1858 (2001)

Sommerfeld, M., van Wachem, B. and Oliemans, R.: Best Practice Guidelines for Computational Fluid Dynamics of Dispersed Multiphase Flows. ERCOFTAC, ISBN 978-91-633-3564-8 (2008)

Sommerfeld, M. and Lain, S.: From elementary processes to the numerical prediction of industrial particle-laden flows. Multiphase Science and Technology, Vol. 21, 123 – 140 (2009)

Sommerfeld, M. and Kuschel, M.: Modelling droplet collision outcomes for different substances and viscosities. Experiments in Fluids, Vol. 57, 187 (2016)

Sommerfeld, M.: Numerical methods for dispersed multiphase flows. In: Particles in Flows (Eds. T. Bodnár, G.P. Galdi, Š. Necčasová), Series Advances in Mathematical Fluid Mechanics, Springer International Publishing, 327 – 396 (2017 a)

Sommerfeld, M.: Lagrangian Modelling of Droplet Collisions in Spraying Systems. Proceedings of the European Combustion Meeting, Dubrovnik, 18. – 21. April 2017 (2017 b)

Sommerfeld, M. and Lain, S.: Numerical analysis of sprays with an advanced collision model. ILASS–Europe 2017, 28th Conference on Liquid Atomization and Spray Systems, 6 – 8 September 2017, Valencia, Spain, pp. 418 – 431 (2017)

Sommerfeld, M. and Pasternak, L.: Advances in Modelling of Binary Droplet Collision Outcomes: A review of available results. International Journal of Multiphase Flow, Vol. 117, 182 – 205 (2019)

Sorianao-Palao, O.J., Sommerfeld, M. and Burkhardt, A.: Modelling the influence of the nozzle geometry on the primary breakup of Diesel jets. International Journal of Spray and Combustion Dynamics, Vol. 6, 113 – 145 (2014)

Squires, K.D. & Eaton, J.K.: On the modeling of particle-laden turbulent flows. 6th Workshop on Two-Phase Flow Predictions, Proceedings, Ed. by M. Sommerfeld, Bilateral Seminars of the International Bureau, Vol. 14, Forschungszentrum Jülich GmbH, 220 – 229 (1993)

Sundaram, S., and Collins, L. R.: Numerical Considerations in Simulating a Turbulent Suspension of Finite-Volume Particles. J. Comp. Phys. Vol. 124, 337 – 350 (1996)

Tennison, P.J., Georjon, T.L., Farrell, P.V. and Reitz, R.D.: An experimental and numerical study of sprays from a common rail injection system for use in an HSDI Diesel engine. SAE Technical Paper 980810 (1998).

Woo, M.W.: Computational Fluid Dynamics Simulation of Spray Dryers: An Engineer's Guide. CRC Press, Boca Raton (2016)

Zaichik, L.I. and Alipchenkov, V.M.: Pair dispersion and preferential concentration of particles in isotropic turbulence. Phys. Fluids, Vol. 15, 1776 – 1787 (2003)

Zhang, J., Mi, J. and Wang, H.: A new mesh-independent model for droplet/particle collision. Aerosol Science and Technology, Vol. 46, 622 – 630 (2012)

Zhang, Z., Chi, Y., Shang, L., Zhang, P. and Zhao, Z.: On the role of droplet bouncing in modeling impinging sprays under elevated pressures. Int. J. Heat and Mass Transfer, Vol. 102, 657 – 668 (2016)